# ACCELERATOR PHYSICS AND INSTRUMENTATION

# THE SOLID HYDROGEN TARGET

A.Zeller, J. DeKamp, R. Fontus, H. Laumer, and D. Pendell

The solid hydrogen target, described previously[1,2], is essentially complete. The target is designed to have an areal density of 10 mg/cm$^2$, but can be changed by additions to the target cell. The target is designed to condense the hydrogen in the cell, then to melt the hydrogen and allow it to refreeze to insure a uniform density. Figure 1 shows a picture of the target.

To test the cell a transparent Mylar window has been installed instead of the intended beryllium foil to allow a visual confirmation of the solidification - melting cycle. The window is held in place with clamping blocks and is glued to insure that it is leak tight. Since the Mylar window is not impervious to helium gas, the window was leak checked with argon.

The target will be tested cryogenically using the CTI 1400 as a source of liquid helium, instead of the 100 l dewar, as soon as the 1400's operational schedule permits.

References

1. A. Zeller, et al, MSU Ann Report 1990, 178.
2. A.F. Zeller, et al, Adv in Cryo Eng 37, 1503 (1992).

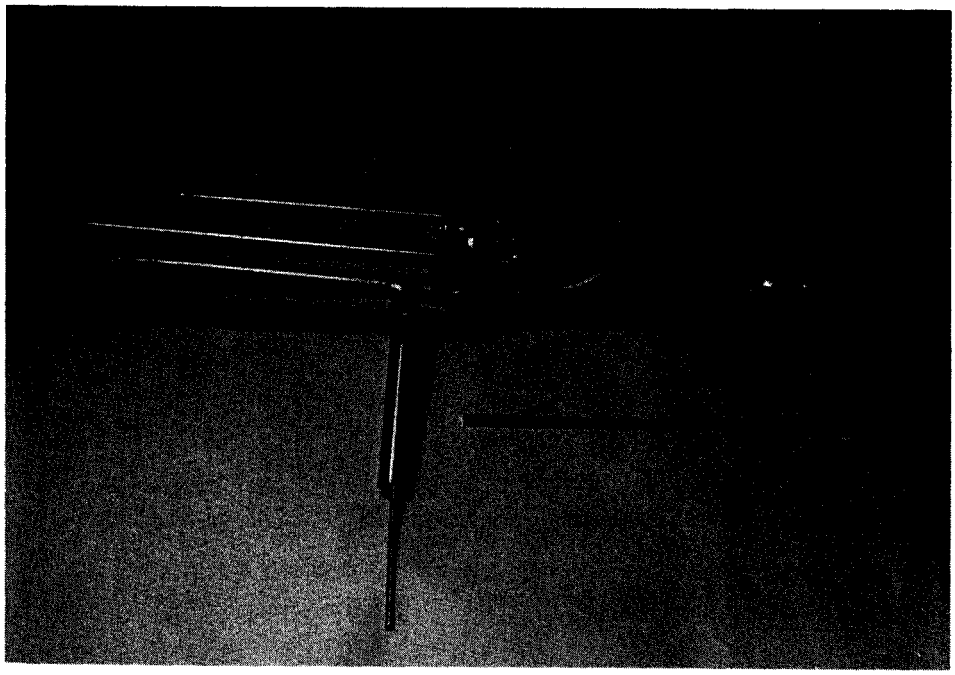

Fig. 1 Photograph of the completed solid hydrogen target with the Mylar test window in place.

# LARGE AREA CsI/PIN DIODE DETECTOR

J. Yurkon, Michael Maier, J.J. Kolata, B. Sherrill and D. Swan.

Scintillation counters are often used as the stopping detector in a telescope due to the expense, and often unavailability, of thick silicon detectors. In order to be useful for particle identification, the detector must be stable. Photomultipliers are one choice to read out the counter, but they must be stabilized due to temperature drifts. A silicon diode / CsI combination is much more stable due to the intrinsic stability of the PIN diode. However, reading out a large crystal can be difficult.

The performance of a PIN diode/CsI detector is not limited by statistics since the quantum efficiency is high, but rather by the signal to noise ratio limitation caused by the high capacitance of the diode. The signal to noise ratio tends to be independent of the size of the diode for a given scintillator. If the size of the diode is doubled, the fraction of light collected is doubled, but so is the capacitance and thus the noise. Therefore subdividing the readout is a better choice. In the case of a 6 x 6 x 4 cm detector, we chose to use four photodiodes. This reduces the capacitance by a factor of four compared to a single detector of equivalent area. Fig. 1 shows the relative areas of the scintillator/diodes combination. This would require

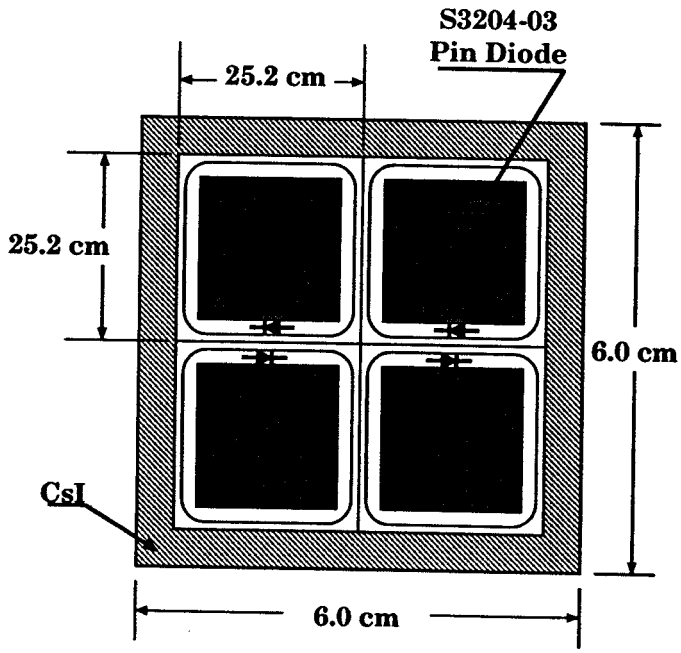


Figure 1: Layout of CsI/PIN diodes.

four channels of electronics for readout however. One of us, Michael Maier, suggested that we wire the diodes in series. This lowers the signal by a factor of four due to division of the signal by the capacitance,

but it also reduces the capacitance by an additional factor of four, so that the resultant signal to noise should be improved by a net factor of four. There is also some gain by the matching of the total detector capacitance to the FET capacitance of the preamp (see fig. 2a). The 1 GΩ resistors are to ensure that the

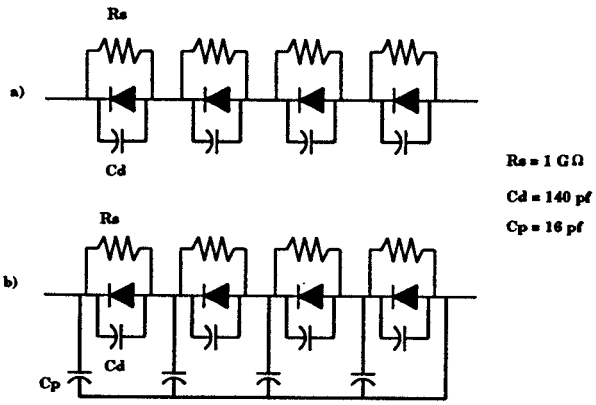


Figure 2: Schematic of PIN diode arrangement.

diodes receive equal bias and contribute about 70 na of leakage current.

We have constructed a detector based on this design, but found it lacking in several respects. First, the reduced capacitance was overwhelmed by the cable capacitance due to the the need to have the preamp far from the detector. With the reduced signal, this actually hurt the resolution. Also we observed an unexplained position dependance of the pulse height that varied by 25%. After reflection, it was obvious that the true equivalent circuit was that of fig. 2b. The parasitic capacitances Cp are due to the cathodes

**Pulse Height vs Position**
**228 Th 8.78 MeV α**

| | | | | |
|---|---|---|---|---|
| 237 | 238 | 238 | 239 | 235 |
| 236 | 238 | 239 | 239 | 235 |
| 238 | 238 | 241 | 239 | 238 |
| 239 | 234 | 239 | 237 | 234 |
| 234 | 238 | 238 | 236 | 234 |

Figure 3: Layout of CsI/PIN diodes.

of the diodes being spaced from the ground plane of the PC board by 1 mm of alumina. This works out to

about 16 pf, enough to explain the observed variation.

We modified the detector by placing the diodes in parallel. The measured response is shown in fig. 3. This is a major improvement and is adequate for its intended use. However, the serial connection of diodes could still be a useful technique if the preamp is placed in close enough proximity to the detector and if there is sufficient space available to separate the diode's cathodes from any ground planes.

# LOW PRESSURE MULTI-WIRE PROPORTIONAL COUNTERS IN A $4\pi$ GEOMETRY

J. Yee, E.E. Gualtieri and D.E. Swan

The construction of low pressure multi-wire proportional counters –(LP)MWPC's– for the MSU $4\pi$ Array is now complete, and installation is currently underway. Previously, the Array consisted of an inner layer of Bragg curve counters in front of a layer of plastic phoswich detectors. In the present configuration, the MWPC's are mounted in front of the Bragg curve counters, forming the innermost layer of the Array.

The frame of the MWPC is constructed of 6 layers of G10 fiberglass with stretched kapton foils (0.3 mil) forming front and rear pressure windows. The anode forms the center layer and consists of a plane of 12 $\mu$m thick gold-plated tungsten wires spaced 1 mm apart. This layer is between two cathode planes which are made of stretched polypropylene foil. (See Fig.1.) A layer of aluminum is evaporated on the

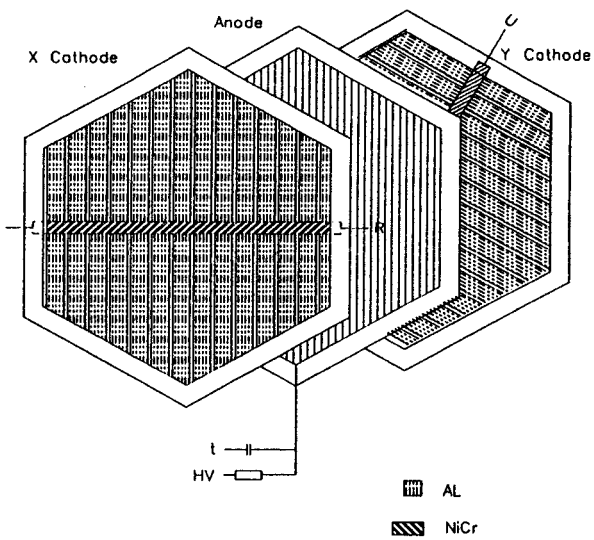


Figure 1: Exploded view of the hexagonal MWPC

surface of the foil, and is divided into 5 mm wide strips connected by a 1 mm wide strip of resistive (5 k$\Omega$) nichrome.[1]

The thickness of the layer of evaporated Al , as well as the thickness of the nichrome layer is 0.1 $\mu$m. Originally, a thinner nichrome strip was to be used, however, problems related to the strength of the strip developed. Any minor stress on the foil caused the strip to crack and the resistance to increase significantly, and so, a thicker strip of nichrome was used in an attempt to defeat this problem. Because of this, the width of the Al strips had to be narrowed to 1 mm in the region where the nichrome strip

crosses them in order to maintain a constant resistivity. Even with these measures taken, the phenomena of rising resistances still remains a concern, but the problem is greatly lessened.

Typically, the MWPC is pressurized with 5 torr of isobutane gas and +500 V is applied to anode. No bias is applied to the cathodes. Ionized charge is collected from both ends of the nichrome strip, and, by using the principle of charge division, information about the position of an entering particle is extracted. By orienting the cathodes such that the nichrome strips cross with a certain angle, we can determine the X-Y position of the particle's punch through point with 1 mm resolution.

While the cathode gives position information, the anode provides a fast timing signal which will serve as a trigger for the BCC's. Without the MWPC, the BCC could only be used as a $\Delta E$ detector for particles that stopped in the first layer of the phoswich. Now, true Bragg Curve spectroscopy can be done, and particles that stop in the BCC can be identified.

References

1. G.D. Westfall, J.E. Yurkon, J. Van Der Plicht, Z.M. Koenig, B.V. Jacak, R. Fox, G.M. Crawley, M.R. Maier and B.E. Hasselquist, Nucl. Inst. and Meth. A238 (1985) 347.

# IMPROVING $4\pi$ ION CHAMBER RESPONSE WITH WAFERPURE FILTER FOR $CF_4/C_2F_6$

J. Yurkon, E. Norbeck, D. Swan and G. Westfall.

$CF_4$ is an attractive gas for use in ionization chambers due to its high stopping power and high electron drift velocity. Other gases, such as $C_4H_{10}$, have high stopping powers but such low drift velocities that for large detectors it causes an ambiguity as to which beam bunch an interaction occurred. However, it has been observed that for this gas the response is sometimes good, sometimes bad. Dr. J. Vavra of SLAC pointed out that it was necessary to purify the gas with a filter to obtain uniform results. It appears that sometimes the impurities have a high electron affinity. One possible contaminant might be flouro-alkynes.

Measurements with an Ion Chamber with a 6.5 c.m. drift volume, and a 0.5 c.m. Frisch Grid spacing were made at various pressures with purified and unpurified gas. The $^{241}Am$ $\alpha$ particles entered the chamber parallel to the electric field. The results are shown in Fig. 1. It is clear that the use of

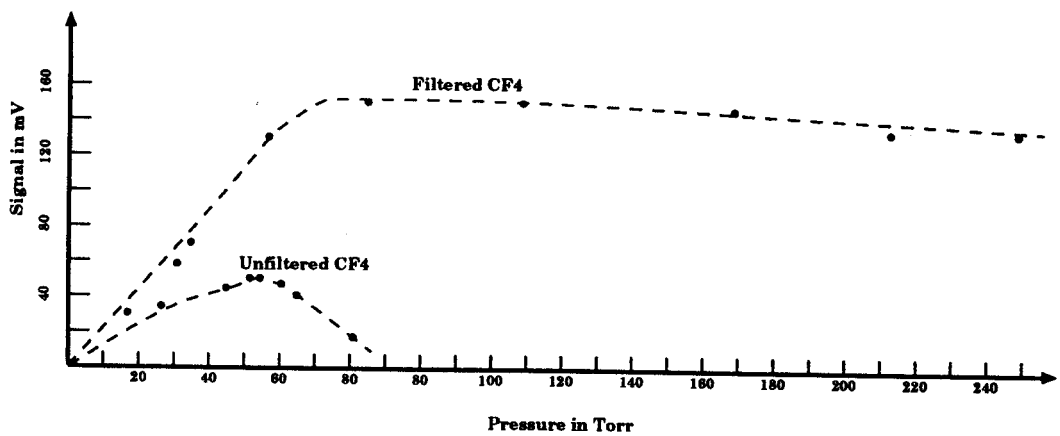


Figure 1: Pulse Height Versus Pressure for $CF_4$.

the WAFERPURE filter makes a dramatic difference. Even $CF_4$ that has been certified of high purity benefits from use of filter. We plan on installing the filter in all systems where $C_nF_n$ gases are used in the future. We also plan to make further measurements where $C_nF_n$ gases are mixed with hydrocarbon gases to see if impurities that do not affect the hydrocarbon gas would cause problems with an admixture of a halocarbon, such as 80 $CF_4$ 20 $C_4H_{10}$.

## References

1. J. Vavra, SLAC-PUB-5728.
2. WAFERPURE Filter, Millipore Corp., Bedford, MA 01730.

# HEAVY ION COUNTER DEVELOPMENT FOR APEX

J. Yurkon, D. Mikolas, E. Kashy, S. Austin, D. Bazin, and J. Winfield.

We have attempted to measure the position resolution of the heavy ion counters for APEX. These counters are position sensitive Low Pressure Multi-wire Proportional Counters that are trapezoidal in shape with an approximate active area of 41W x 13W x 54L c.m. The detectors cover a laboratory angle of 50deg. The experiment setup was a 200 MeV $^{58}$Ni beam on a $^{58}$Ni target in the APEX vessel. The detectors were filled with 6.0 torr of $C_4H_{10}$ and operated at 610 Volts bias.

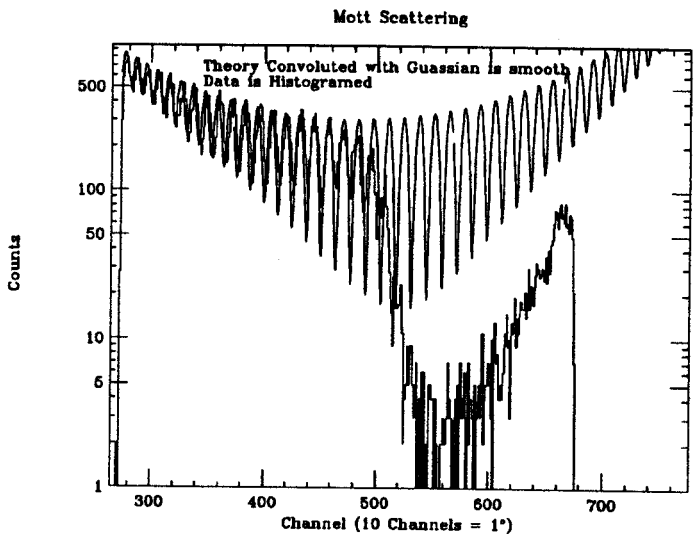


Figure 1: Pulse Height Versus Pressure for $CF_4$.

Identical nuclei at subcoulomb barrier energies have a resonances in the scattering cross-section known as Mott Scattering. These are easily calculated and used as a calibration and determination of the resolution of the counter. In Fig. 1 we have plotted the theoretical Mott Cross-section over the measured spectrum. The plotted cross-section has a 0.25deg FWHM gaussian convoluted in and includes the effective solid angle of the detector. As can be seen, the curves match well implying that 0.25deg FWHM is the resolution of the counter. This is at the narrow end of the counter where the delay/angle is the smallest and the resolution requirements are the most stringent. Since this resolution is adequate we have met our design goals. Above channel 400, where the curves no longer match as well, is the region where the Ni has insufficient energy to completely penetrate the detector due to the kinematics. With 6MeV/n $^{238}$U this will not be a problem.

# IMAGE INTENSIFIED CAMERA FOR BEAMLINE DIAGNOSTICS

J. Yurkon, W. Benenson, F. Marti, J. Nolen and B. Sherrill.

Diagnostics of radioactive or secondary beams can be difficult due to low production. Ordinary scintillators viewed by a standard TV camera often do not provide an intense enough image for viewing. Still, the rate can be too high for conventional imaging detectors. An image intensified camera, such as the XYBION ISG-250, viewing a rare earth phosphor can fill in the gap between imaging detectors and normal TV cameras. The ISG-250 has a sensitivity of $1.0*10^{-7}$FC faceplate illumination. It was recently

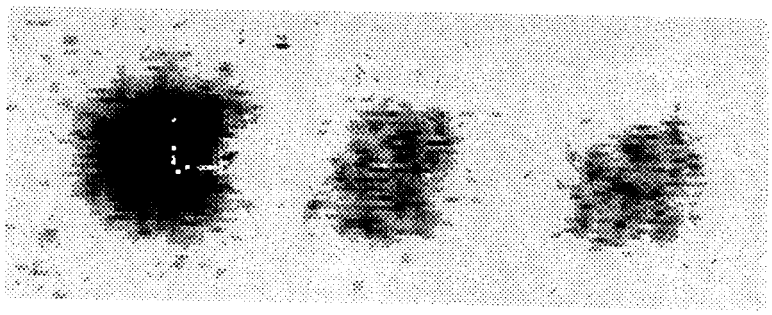

Figure 1: $^{38}$Ar(100 MeV/A) on Be. Beam spot 8 mm full width.

used to focus the image in the Analysis Line where the production was $^{38}$Ar(100 MeV/A) on Be. In Fig. 1 one can see, from left to right $^{37}$Cl, $^{35}$S and $^{33}$P. The total intensity was about $10^3$c/s.

The camera will have other uses, such as imaging wire chamber discharges and possibly as a focal plane detector with time of flight capability.

## References

1. Xybion Electronic Systems Corp., 8380 Miralani Dr., San Diego, CA 92126-4347
2. Private communication with B. Sherrill

# NARROW EDGED PIN DIODE FOR BEAM LINE DIAGNOSTICS

J. Yurkon, F. Marti, J. Bailey, J. Nolen and J. Ottarson

Previous diagnostic tools for measurement of beam timing were hampered by the problems of not being able to measure the time of individual particles in a bunch and of not working well in the internal region of the Cyclotron. We hope to solve these problems by using a PIN diode that has an active region that extends to the edge of the detector. It is necessary for the active area to extend to this region since the beam must not intercept the detector in an orbit before it is detected.

Fabricating a detector out of silicon without a dead region at the edge is difficult. Normally, guard rings or other structures are used to terminate the active region to reduce leakage currents to manageable

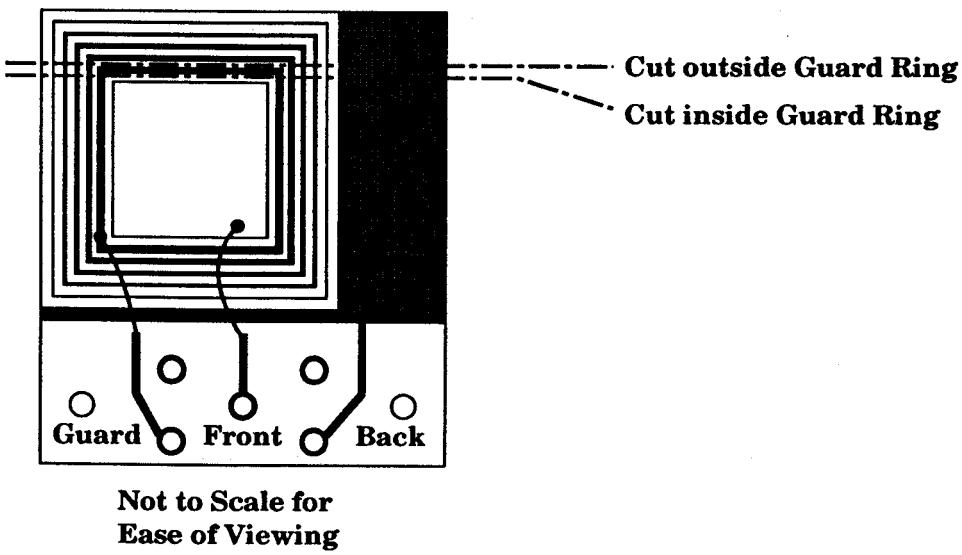


Figure 1: View of PIN Diode.

levels. Senter for Industriforskning has produced three detectors for us. One had a normal structure for comparison, another had only one guard ring, and another had no guard ring on one edge as shown in Fig. 1. Leakage currents were measured before cutting (Table 1) and mounting and then again after cutting

| Device | Bias Voltage | Active Current | Guard Current |
|---|---|---|---|
| Uncut | 40 V | 65 pA | 650 pA |
| Cut Outside | 50 V | 35 pA | 509 pA |
| Cut Inside | 50 V | 65 pA | 560 pA |

Table 1: Measurements Prior to Cutting.

(Table 2) and mounting. It would appear that the device that was cut just outside the first guard ring will

| Device | Bias Voltage | Active Current | Guard Current |
|---|---|---|---|
| Uncut | 40 V | 1.3 nA | 2.4 nA |
| Cut Outside | 35 V | 38 pA | 18.0 $\mu$A |
| Cut Inside | 40 V | 4.0 $\mu$A | 4.3 $\mu$A |

Table 2: Measurements after Cutting and Mounting.

be usable. We currently have built a probe to hold the device and plan on tests in the near future. SI also informs us that they may be able to optimize a device by implementing the field termination as part of the active diode. We need to fully characterize the present devices first however, before proceeding further.

## References

1. Senter for Industriforskning, P.O. Box 124 Blindern, 0314 Oslo 3, Norway

# USES OF UNIX AT NSCL

R. Fox, A. VanderMolen, R. Au, F. Marti, T. Antaya, D. J. Morrissey, W. Bauer, M. Thoennessen, W. Lynch, and B. Tsang

## Introduction

In the last three years, the UNIX(TM) workstation market has expanded greatly. As new and faster computer systems come out at an ever increasing pace, the ease with which UNIX can be ported to different platforms makes it the operating system of choice for these "hot" boxes. In addition, the services of the UNIX operating system are the basis for the current set of national and international standards for operating system call interfaces (POSIX). As a result of these trends, physics laboratories have been increasingly augmenting their traditional VAX/VMS computing environments with workstation level UNIX systems.

This article describes the role of UNIX computing systems at NSCL. In this article we will:

- Describe UNIX computing resources currently available to NSCL staff.
- Describe the uses to which the UNIX computing resources are currently being put.

We round out the article with an assessment of the success with which UNIX systems have been integrated into the NSCL computing environment and some thoughts about the roles that we feel that UNIX systems will play in the future.

## Unix resources at NSCL

The UNIX systems at NSCL make up a heterogenous network of computers. This network is bound together loosely with file sharing, printer sharing, file transfer and remote access. This section describes the types of computers which participate in this network and the mechanisms by which remote resources are accessed and shared.

The UNIX systems at NSCL are heterogeneous. Currently we have systems provided by Intergraph, Digital Equipment Corporation, SUN, NeXT, and Mega (a high end I.B.M. PC clone maker). These systems represent the three major dialects of UNIX: Berkeley Standard Distribution (BSD), AT&T System V (SVID), and Mach with BSD emulation. In addition to the systems in the table, a Tatung

Table 1: Breakdown of Unix workstations at NSCL by vendor

| Vendor | Model | Quantity | UNIX Dialect |
|---|---|---|---|
| DEC | DS500/200 | 2 | BSD |
| SUN | SPARCstation ELC | 1 | BSD/AT&T |
| NeXT | NextStation | 3 | Mach |
| InterGraph | InterPro 120 | 6 | SVID |
| Mega | 486 50Mhz | 1 | SVID |

COMPSTATION 40 (SPARC clone) is currently on order and will have arrived by the time this article is in print.

The Unix systems share files both with each other and with the VAX/VMS cluster. The software used to accomplish this is NFS. One of the DECstations serves as a file server. The VAX/VMS cluster exports both VMS disks and some additional pseudo UNIX disks via the DEC Ultrix Connection (UCX) product.

UNIX users typically would like to have access to all printers that are available at NSCL. On the VAX cluster, this is done using a combination of cluster wide print queues to support distributed queueing and placing the printers on ports of LAT terminal servers. Thus each printer has multiple queues pointed at it, with the terminal server arbitrating access. If users submit jobs to generic queues which are served by these queues, then they have a fault tolerant printing system. Not all UNIX systems are capable of printing via LAT terminal servers, however. Therefore, the DEC systems are used as printer servers. All other systems use remote lpd accesses to remotely submit print jobs through these systems. While the remote lpd system does not support a fault tolerant queueing system, nonetheless, if the server node is down, the job is not lost, only delayed.

File transfer augments file sharing. In some cases, a desired file may not be on an exported VMS or UNIX volume, or the user may want to make a local copy to support high speed access. This can be done using the TCP/IP file transfer program (ftp) available on all systems. In addition, the DEC workstations support DECnet file transfers.

Remote system access is handled through either of two mechanisms, depending on the desired functionality. Telnet supports a simple terminal login session to a remote system. UCX on the VAXcluster includes a bi-directional telnet implementation. This allows users on any system to log in to any other system. The DEC workstations, in addition, support both LAT and DECnet. All of the workstation systems

in the lab are X-windows systems. This means that programs which have graphical needs, or make use of a graphical user interface, can be displayed from remote computers.

### Accelerator Physics and moviemaking

The K-1200 cyclotron is outfitted with a T.V. viewer probe. The radius of the scintillator being viewed can be altered. The result is a very detailed profile of the beam as a function of radius. Computations of equilibrium orbits provide a tool for understanding and to some extent recreating some of the structure that is observed in the real beam. A detailed understanding of these structures can lead to improved accelerator tuning methods as well as suggest upgrades to the system which improve overall operation. F. Marti has written code to produce a simulation of viewer probe images from the results of existing equilibrium orbit calculations. The reproduction of each image is a time consuming process. When run on a DECstation 500/200, a rate of approximately one frame a second can be achieved. If these frames are computed and displayed in real time, the result is a rather jerky computer generated "movie." Comparing these movies with video tape taken from actual probe traces under similar conditions tests how well the beam is being modelled by the equilibrium orbit code.

### The ECR and IBM P.C. workstations

The most recent addition to the set of UNIX systems at NSCL is an Intel 486 50Mhz SCO Unix based system. The system runs Open Desktop which is SCO's implementation of X-windows with the Motif window manager. X-windows coupled with OSF/Motif is rapidly becoming the NSCL standard windowing system. This system was acquired to perform plasma and beam simulations for the NSCL ECRs. T. Antaya plans to port an ion source beam extraction code called Beam3d. At present this program requires 4-8 hours of execution time on a 4 Specmark system (VAX 8530). It is hoped, based on relative benchmarks between existing VAX/VMS systems and the 486, that Beam3d's run time can be cut to an hour or less. Once this and other simulations are ported to generic UNIX Fortran, it will be possible to take advantage of higher performance Unix computing resources as they become available.

### NeXT stations and document preparation

At present, almost all technical journals accept articles submitted in LaTeX format. Those that do not will accept camera ready copy which is often most easily produced using TeX and LaTeX.

These markup language systems are very flexible but have some drawbacks. The process of converting from input to device independent (DVI) format and then of converting to a device dependent format is quite compute intensive. The fact that LaTeX and TeX are markup languages also means that it is important to be able to preview the output several times prior to making final printouts or submissions.

Low cost Unix workstations with high resolution graphics display systems are ideal for this sort of operation. Documents can be prepared, edited and previewed with a very good turnaround time. The high speed, high resolution displays of these workstations make them ideal as preview engines.

Two of the three NeXTstations that have been purchased are used extensively in this role. The graphical object oriented nature of the NeXT Step user interface makes these systems very capable electronic publishing systems.

### UNIX workstations in nuclear physics

The main mission of NSCL is nuclear physics research. Here too, UNIX workstations are becomming valuable tools in data analysis, simulations and theoretical computation. All of these areas are highly compute intensive. Reducing the time required to complete each calculation clearly enhances productivity. In addition, graphically displaying and exploring the results of these caclulations allows the scientist to get a better handle on the patterns and anomalies present in the data.

One of the more important tools in the theoretical physicist's arsenal are computer programs which perform symbolic mathematics. The premier package in this area is probably Mathematica. For example one of the ways that W. Bauer uses Mathematica on a NeXTstation is to solve pion-pion scattering wave functions. The results of these computations can be displayed graphically, explored from various viewing angles and pasted into papers that are under preparation. The NeXTstations, while not a very high performance compute system, provide very good graphics support for the visualization parts of Mathematica.

Simulations of nuclear reactions are being performed by a number of people at NSCL. M. Thoennessen runs Monte Carlo programs to simulate proton/neutron coincidence measurements. The two programs, a statistical model program based on PACE[1] and a RAYTRACE[2] based ray tracing program are both run on DECstation-5000's. The results of these simulations are a tool to understand the data that has been taken as part of his experimental program.

On another front, BUU and QPART are being used to simulate nuclear reactions in support of the Miniball experimental program. These simulations are run on both of the DECstation-5000 systems. Results enhance the understanding of data taken in the runs of that detector.

UNIX workstations are used in a few data analysis roles. M. Thoennessen has brought up the Oak Ridge ORNL/HHIRF data reduction system on the NSCL DECstation 5000's and is using this package to analyze data taken at ORNL last year. A. VanderMolen and S. Hannuschke are currently doing preliminary analysis of pion data taken from the $4\pi$ Array on the DECstation 5000 systems. Several of the simulations which have been mentioned earlier in this section are in support of the analysis of various experiments. D. Morrissey is presently beginning late phase analysis of data taken from half life experiments performed at NSCL using a NeXTstation.

### UNIX and Data Acquisition

At present, no data acquisition is being performed on UNIX workstations. This is expected to change in the next year or so. Pieces of the NSCL data acquisition system have already been ported to UNIX systems including the DECstation 5000's and SUN systems. At present the following software has been completely ported or written:

1. ROUTER - the program responsible for distributing data acquired by a single computer to multiple processes within that computer.[3,5]
2. An ETHERNET event source for ROUTER which receives data from the NSCL front end systems[4]

Work is underway to port the NSCL tape logging program to UNIX. When this is completed, a minimal core data acquisition system will be available for UNIX users. We hope to test this minimal core system in $4\pi$ Array runs scheduled for August of this year. The minimal core system will be extended with on-line data viewing software as well as data analyzers. The whole system will be controlled via a graphical user interface that will be built from the X-windows display system and Motif toolkit libraries.

### Conclusions and Directions

For the most part, UNIX workstations have been successfully integrated with the remaining NSCL computers. There are some areas, however, where there is room for improvement. In particular, the file

sharing between UNIX systems and VMS provided by the UCX product is not very good. If the file was originally created on the VAX, it is sometimes easier to use file transfer rather than file sharing. This is due to the rich set of file and record types available in VMS.

Within the UNIX domain itself, the systems from each vendor have system management methods which are similar enough to make you believe that they are the same while being different enough to let get you into trouble. The same is true of the tool programs seen by the users. In this area there are two pitfalls:

1. The commands will accept different sets of switches for each UNIX dialect.
2. Commands will be located in different parts of the filesystem tree depending on the dialect of UNIX.

These concerns make it very difficult to glue together a mixed vendor UNIX environment as tightly as a VAXcluster running VMS. NFS and NIS are big helps here but it seems to always be necessary to throw some symbolic links in here and there to fix things up.

In the future, it is very likely that the use of UNIX at NSCL will increase. This will be driven by the price performance curve and the increasing use of UNIX based systems for undergraduate computer programming courses. Until the NSCL UNIX software development effort gathers a critical mass of software, usage is likely to remain confined to compute intensive codes and use of packaged software.

Within one or two years, however, we hope to have a UNIX based distributed data acquisition system running. We would also like to have a set of tools for data analysis available and running. Using graphical user interfaces based on X-11/Motif and the POSIX standards should allow this software to port very easily from system to system.

## References


1. PACE A. Gavron Phys. Rev. C21, 230 (1980)
2. RAYTRACE S. Kowalski, H.A. Enge, MIT (1987)
3. A multitasking multisinked multirprocessor data acquisition front end R. Fox, R. Au, A. VanderMolen IEEE Trans on Nucl. Sci. NS36-5 1562 (1989)
4. A network protocol for data acquisition at NSCL R. Fox, R. Au, A. VanderMolen IEEE Trans on Nucl. Sci. NS36-5 1608 (1989)
5. Progress on the Data Acquisition system at NSCL R. Fox, R. Au, A. VanderMolen, B. Pollack, T. Glynn IEEE Trans on Nucl. Sci. NS32-4 1286 (1987)

# PROGRESS OF THE PARALLEL PROCESSING DATA ACQUISITION SYSTEM

A. Vander Molen, R. Au, R. Fox and D. Tantalidis

Experiments at NSCL are being run with an increasing number of parameters and higher statistics. In certain cases this strains or will strain the limits of the current data acquisition system. For example both the $4\pi$ Array and the Miniball detector fall into this catagory. Each of these detectors house hundreds of elements and with near $4\pi$ coverage. Both are also in the process of adding more elements. In the case of the $4\pi$, with the addition of the new forward arrays, data rates could reach 1 megabyte/sec. The current limits of the acquisition system are closer to 300 kbytes/sec. A good percentage of the data may not be of value – noise or redundent information such as FERA headers. In the case of the $4\pi$ this percentage is close to 30 percent. Because of this, there is a need to acquire data at higher rates and reduce or filter those data before permanently storing them. A study has been undertaken to determine the feasibility of using parallel processing at NSCL for this purpose. The early emphasis of this work is on a real time filter for the $4\pi$ Array using inmos transputers; the T800 series at first and later upgrading to the T9000 series.

The transputer, in addition to being a high speed computer, is ideally suited for parallel processing. Each transputer chip has 4 high speed communications links, each of which can be connected to other transputers or other devices through link adapters. Because these links are built into the chips, networks of transputers can easily be constructed from transputer modules by simply cabling the links together. The language, OCCAM, used to program these chips has all the necessary tools to easily take advantage of parallelism. Parallel C and FORTRAN are also available.

The first feasibility test that was done emulated filtering on the $4\pi$ data acquisition front end. This was done by processing a $4\pi$ data buffer read from the CES 8170 memory board. The Process consists of two parts. The first part is to combine the various data for a particular particle into one contiguous stream. This will eliminate redundant FERA header information and make future analysis easier and faster. The second part is to eliminate unidentifiable particles, i.e., those with no $\Delta E$ signal. Previous analysis has shown this filter algorithm would reduce the data set by about 30 percent. Using a single transputer housed on a VME board, a program was written to read, filter and send data via a link at rates on the order of 260 kilobytes/sec. Current data rates to tape using the MC68020 based data acquisition are on the order of 280 - 300 kilobytes/sec. The conclusion drawn from this is that a single node transputer

system could act as a simple real time filter and improve the overall preformance of the acquisition system. Additionally, with the appropriate number of nodes, a sophisticated real time filter could be constructed.

Currently, plans are under way to build a transputer based system for the $4\pi$ Array. This system would consist of a VME-based transputer linked to a SUN-clone workstation. The workstation would be used for system control, data recording and online displays. The workstation would also have the NSCL routing system so other workstations could receive data. The filter algorithm will consist of the aforementioned filter plus a particle mutiplicity filter. Currently, hardware alone is being used to take events of a given or higher multiplicity. However, this is in reality a "hit" multiplicity. The transputer filter would be used to count the identifiable particles and eliminate those events that do not meet the required level. Once this is completed, research will be on the implementation of a multinode system or farm. Investigations are also going on in the area of using TRAMs. These are boards that have a transputer or a transputer link on them along with an another device or devices such as ADCs or Ethernet. The concept being entertained is to have TRAMs on the detectors themselves and then to network them together via the links. Each node would then read and filter the data from its module in parallel and transmit the data via links to the "harvester". The harvester could pass the data to a farm of transputers for higher level filtering and/or recording. These TRAM nodes could ultimately be trained, as in neural networking, to make decisions as to the quality of the data from the individual detector that it is monitoring. This in turn could lead to physics data being generated in real time, greatly improving the quality of the data and reducing the post-experiment data reduction time.

# A LIQUID HELIUM CRYOPUMP FOR THE 92" SCATTERING CHAMBER

D. P. Sanderson

As larger arrays of detectors have been installed in the 92" Scattering Chamber, the vacuum requirements have grown. Until recently, they were satisfied by two large turbo pumps and a liquid nitrogen cooled trap. However the volume occupied by the trap is now needed for detector arrays. A larger turbo pump is uneconomical. Therefore it was decided to combine the two by fabricating a liquid helium cryopump. This freed up both the volume in the chamber occupied by the cold trap and a large capacity turbo pump. Since it is plumbed into the laboratory cryodistribution system, the new pump's speed and capacity is limited by the conductance of gas to its cold surface and the refrigerating capacity of the laboratory's main helium liquifier.

A schematic of the pump is shown in figure 1. The liquid helium dewar is a stainless steel 87 liter vessel with a level sensor and two calibrated resistors for instrumentation. An opening at the bottom exposes the liquid through a bimetal plate to an oxygen free high conductivity copper pumping surface which completely surrounds the dewar. Since the copper shell only touches the dewar at the open port to the liquid, the copper stays the same temperature regardless of liquid level. The front of this shell is the main pumping surface for air molecules. The boiloff gas is passed through a gas cooled shield between the dewar and the liquid nitrogen container. This shield operates between 4.2K and 77K to reduce boiloff in the dewar. In turn, it is surrounded by a rectangular stainless steel liquid nitrogen vessel. The vessel holds 92 liters with a two position level controller for automatic filling. The liquid helium dewar is protected from room temperature radiation by the gas cooled shield and a copper chevron attached to the bottom of the liquid nitrogen dewar.

A mechanical pump is valved to the cryopump and interlocked such that if the internal pressure rises above 100 mTorr, (as during warmup) it pumps out the adsorbed gases. The cryopump is connected to the scattering chamber through a 20" bore stainless steel gate valve. Table 1 compares the pumping speeds of the cryopump and the turbo/cold trap combination it replaced. Although the cold trap pumped water faster, its loss freed up a very valuable area inside the chamber.

**Table 1.**

| | Cold trap + Turbo | Cryopump |
|---|---|---|
| Pumping Speed: | | |
| Air | 1375 l/sec | 4431 l/sec |
| Water | 97,500 l/sec | 22,100 l/sec |

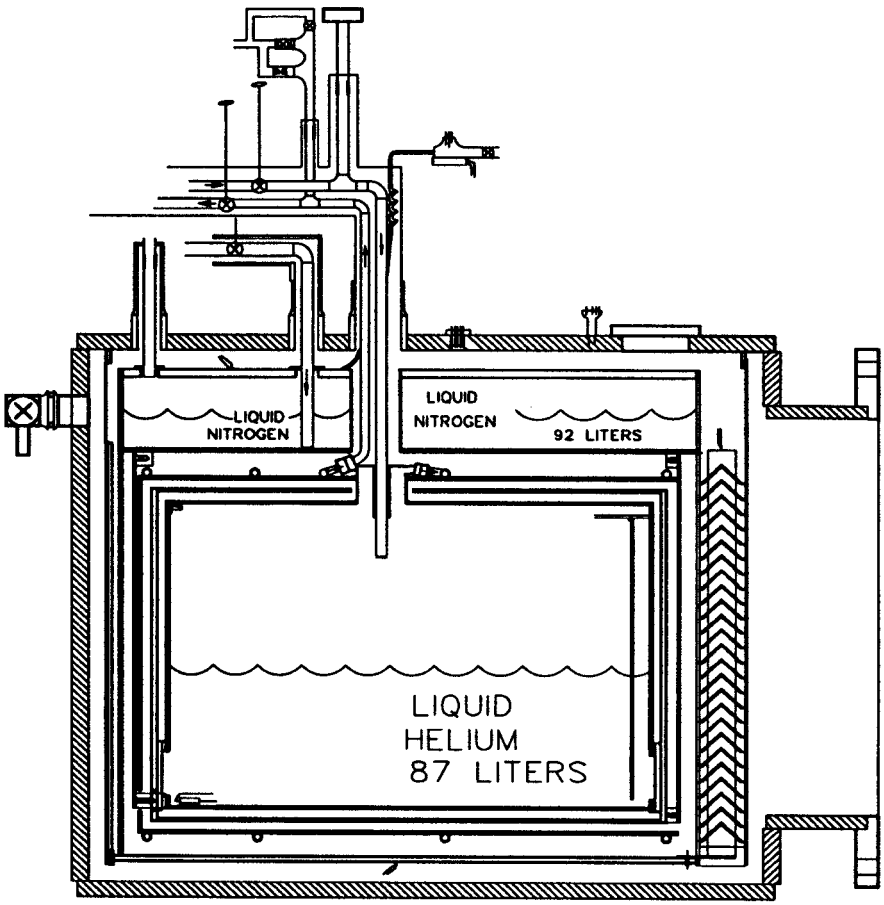
LIQUID
NITROGEN
LIQUID
NITROGEN
92 LITERS
LIQUID
HELIUM
87 LITERS

**Figure 1.**

# A COMPUTER BASED MONITORING SYSTEM FOR THE CRYOGENICS SYSTEMS AT NSCL

D. P. Sanderson and H. Laumer

The cryogenic system at NSCL has grown through the years to become large and complex. It has become necessary to provide a means of monitoring and controlling the condition of the refrigeration system and the helium levels of the large number of superconducting magnets at the facility. To this end, we have assembled a system which optimizes the production of the refrigerator and monitors the cryogenic status of the liquid helium reservoirs in the laboratory.

Figure 1. shows a schematic of the system. At its heart is a "PC compatible" 386SX-16 computer. It holds the analog to digital board, a digital to analog board with digital I/O, and the two communications boards which interface with the laboratory's main control system and the mainframe which stores the data. The ADC board monitors voltages located near the refrigerator. These include level sensors and pressure transducers. The DAC board is used in a feedback loop to control the wet expansion engine in the refrigerator. The digital I/O opens and closes control valves to regulate the liquid level in the K1200 cyclotron. An RS-232 communications board talks to the main control system to monitor the liquid levels in the beamline magnets. An ethernet board is used to send the accumulated data to a UNIX mainframe which makes the information available to anyone who logs in. The instantaneous data is displayed on a monitor in the cryogenics area.

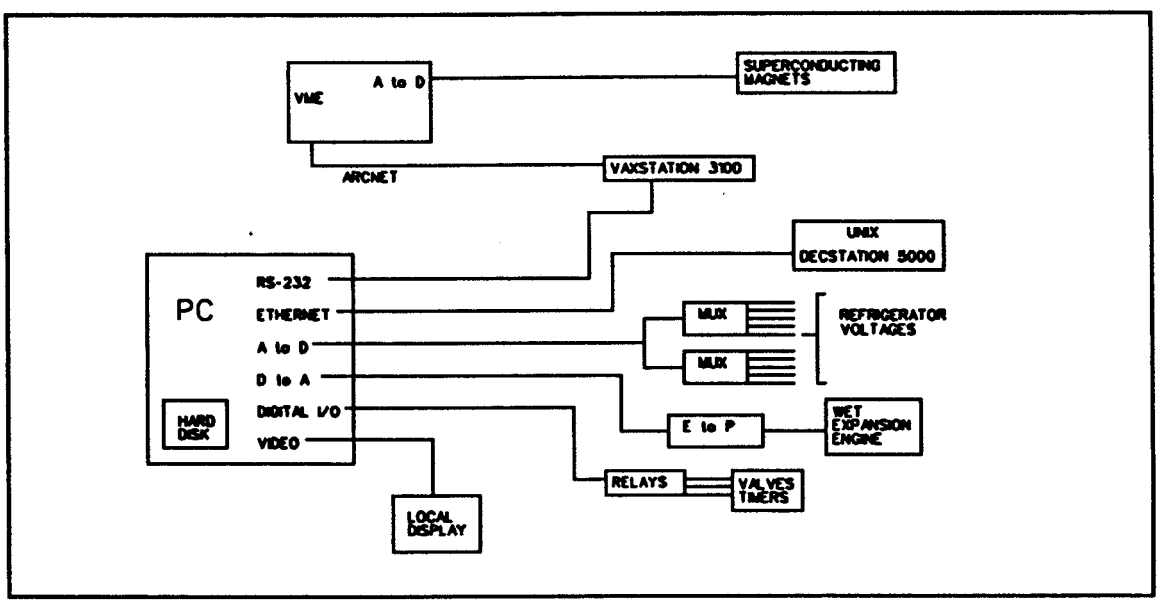


Figure 1.

To keep the costs low, we chose Keithley/Metrabyte DAS8-PGA 12 bit analog to digital boards which mount inside the computer. This application has a low sampling rate with a required resolution of 1 part in 100. By multiplexing the channels, up to 128 voltages can be read. We use one multiplexer with a gain of 2 for high level (0 to 5V) signals and another with a gain of 100 for the low level signals(0 to 100mV) which come from the recorder outputs of instruments such as helium level sensors.

The speed of the wet expansion engine on the refrigerator is controlled by the computer. A tachometer returns a voltage proportional to speed. The computer carries out a proportional-integral-derivative (PID) calculation and generates a correcting voltage through a Keithley/Metrabyte DDA-06 digital to analog converter. This voltage is converted to a pressure by a Fisher E to P unit. The pressure regulates a hydraulic brake on the engine drive shaft. This system keeps the engine speed constant during changing pressure conditions in the refrigerator heat exchangers.

One of the DDA-06's digital I/O lines controls a valve on the liquid line to the K1200 cyclotron. The computer monitors the liquid level in the lead port of the cyclotron and cycles the valve between low and high flow to keep the liquid level within a small range. To ensure that the system has not been "hung" by communications errors to the mainframe, one of the digital I/O lines is cycled every five minutes. This resets a timer watchdog relay controlling the power to the computer. If the line is inactive, the computer is rebooted and the program restarted to clear the problem.

The sytem takes a complicated path to retrieve the beamline magnet levels. Once every three minutes, the Modicon programmable logic controller system energizes the level sensors. It signals the VME control system that the voltages from the sensors are valid. Once a second, the Vaxstation 3100 asks the VME if the data is valid. If it is, the station collects a copy. Once every ten minutes, the refrigerator monitoring PC sends a request down an RS-232 serial line for the most recent valid data. This data is displayed on the monitor and logged.

Inside the PC, data is recorded once a minute to a file on its internal hard disk which is erased once a day. This file is useful if something breaks since it monitors short term trends. The data is recorded to the internal disk once every ten minutes in files which are date stamped and saved. A copy of the ten minute data files (refrigerator, beamline) is transfered to a UNIX based Decstation 5000 minicomputer over a ethernet cable using Sun's PC-NFS networking software. This makes the data available to an interested party elsewhere in the laboratory or at home.

In the cryo-vac area of the laboratory, the instantaneous data is displayed on a high resolution (1024 x 768 pels) screen using fortran callable graphics routines. The high density of information allows all of the data collected to be displayed on a single screen.

We believe this system has worked well at monitoring and logging the cryogenics systems of the laboratory. In the near future, we expect to expand the control functions to the other expansion engines and the K500 cyclotron.

# RF COUPLER INSULATOR FABRICATION AT NSCL

D. P. Sanderson and G. Stork

A critical part of the RF system of the cyclotrons at NSCL is the feedthru which passes RF power from the transmitter to the vacuum inside the accelerator. The feedthru presently used in the K1200 consists of a small alumina ($Al_2O_3$) ceramic insulator which must be joined to two copper rings. In the past, the part has been custom fabricated by a commercial ceramic firm, which charged high prices with long delivery times (6 mo.). This made it extremely difficult to try new ideas in a timely manner. Therefore we decided to purchase a large number of simple insulators and join them to the copper parts using the brazing furnace facility at NSCL.[1] The main thrust of this research program during the past year has been the fabrication of coupler insulators which incorporate "greyed" alumina.

A "greyed" alumina is one in which iron oxide impurities have been reduced to metallic particles inside the ceramic. This reduces the surface resistivity as well as the secondary electron emmision from the alumina. It is hoped that this will increase the lifetime of the couplers.

We start with a purchased ceramic ring of either 94% or 99.5% alumina[2]. Although the delivery time of the ceramic is long, we save a factor of ten in price when compared to a complete assembly. Once a large stock of ceramic is in-house, the turnaround time for a new design is approximately one week, including fabrication of the copper pieces. The 94% alumina is brown when it arrives. The surface is "as ground" to the precise dimensions needed. The seal area is metallized using the "moly-manganese" process in a wet hydrogen atmosphere. This changes the ceramic color to pink. After cooling, the ceramic is heat treated at a temperature 250° below the metallization temperature in a dry hydrogen atmosphere. This "greys" the alumina to a brownish pink color. The 99.5% alumina arrives white and turns only slightly grey after metallization and heat treating. The metallization layer is nickel electroplated using a "watts" type bath for good adhesion to the brazing alloy. Finally the ceramic is joined to the copper parts using copper-silver eutectic alloy at 800° C in a spacing fixture. Helium spectrometer leak checking is used for quality testing. Once the assembly is leak tight, it is attached to the rest of the coupler assembly and tested again.

At present two designs of coupler insulator are in use on the K1200 cyclotron (See fig. 1). The planar coupler insulator is fabricated using 99.5% alumina. It was purchased factory metallized and nickel plated. A "greying" style heat treating would destroy this layer, so the part was joined as delivered. We simply brazed it to the copper parts using an alloy of 15% Pd, 65% Ag, and 20% Cu. This alloy fills cracks in the joint better than the copper-silver eutectic normally used for such joints. Since the copper expands away from the ceramic when heated, we wrapped bands of molybdenum sheet around the outside of the joint area with molybdenum wire to hold the assembly tight.

The first attempt at using a "greyed" insulator used a 99.5% alumina cylindrical insulator. After metallizing using type HT-1WH paint[3] at 1450° C in a wet (dewpoint=25° C) hydrogen/nitrogen

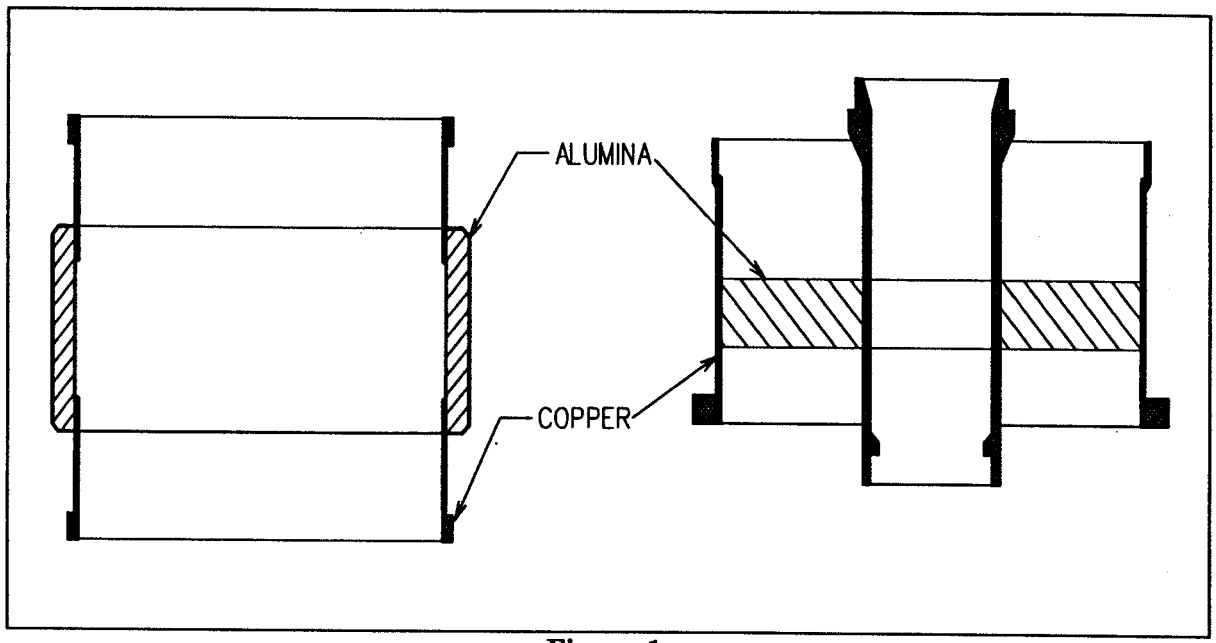


**Figure 1.**

atmosphere for 1/2 hr., the part was cooled and then "greyed" in a dry hydrogen/nitrogen atmosphere at 1450° C for 3 hours. Although the metallization layer appeared intact, after plating and joining to the copper pieces, the layer failed. It appears that the long period at high temperature without water vapor reduced the glassy phase of the manganese oxide in the metallization layer to metallic manganese, breaking the joint. The next attempt was to try to join the "greyed" alumina to the copper using an active metal brazing technique. Cusil-ABA alloy,[4] which has 1.75% titanium as a constituent, was inserted into the joint and heated in a vacuum to the liquidus temperature. The joint failed to adhere to the ceramic. A likely cause of the problem was oxidation of the titanium in the residual gas of the vacuum system. In the future, we will use titanium metal screws placed around the joint to react with the residual oxygen instead of the brazing alloy.

Because of the above problems with the high purity alumina, we decided to try the techniques on a 94% alumina (pink). The ceramic was metallized using type HT-2MH paint[3]. The heat treating could be carried out at a much lower temperature (1200° C) for this alumina. After nickel plating, the insulator was joined to the copper pieces using the copper-silver eutectic alloy. This time the joint was leak tight. The assembly was incorporated into a coupler and installed in the cyclotron.

The next step in this project is to fabricate more spare cylindrical insulator assemblies using the successful procedure outlined above. After we have sufficient spares, we will try the procedure on new planar 94% alumina insulators. The active metals process needs more development to perfect a procedure for the "greyed" high purity alumina ceramic. We are presently expanding this program

to include ceramic joining projects from other areas of the laboratory. The facility is proving to be both cost effective and quite beneficial.

## References


1. NSCL Annual Report 1989, p. 245.
2. 94%: Frenchtown Ceramics #4462. 99.5+%: Wesgo type Al998.
3. International Technical Associates.
4. Wesgo, Inc.

# PHOENIX POWER SUPPLY UPGRADE

William Nurnberger and John Vincent

The Phoenix power supply provides anode power for the K1200's RF amplifiers. As a matter of reference, its name was recently changed from the Aydin power supply to the Phoenix because it has risen from the ashes of the original Aydin Energy Systems power supply so many times that there is actually very little left of the original Aydin components. Over the past two years the Phoenix has undergone one major revision to its control and DC power distribution equipment and is presently in the midst of another major modification to the AC power, rectifier and filter systems.

In the Aydin supplied equipment, all the control equipment was housed in a large cabinet which also contained the crowbar switch and the high voltage DC distribution equipment. Although most of the control equipment is relay based and is thus relatively insensitive to ground and inductively coupled surges associated with the HVDC, the same was not true of the crowbar trigger and monitor circuitry, which is low level, relatively fast solid-state circuitry and decidedly not surge proof. The surge problems were complicated by the lack of a well defined DC return path (and, sometimes, source path - hence the name change) for the anode currents, and an almost completely undefined fault or crowbar surge return path.

It was decided to re-design the DC high voltage distribution cabinet using a semi-microstrip approach to provide a well defined ground return path for both the DC and higher frequency components of the the DC return currents. The new distribution cabinet is a large NEMA-12 style cabinet with doors on the front and rear. The front of the cabinet is separated from the rear by a metal plate which is insulated from the cabinet everywhere except the top edge, where it is joined to the ground terminal plate which also serves as the top of the cabinet. This insulated metal plate serves as a ground plane on which all the high voltage components are mounted. The high voltage DC from the rectifier/choke enters the cabinet through the top ground terminal plate toward the rear of the cabinet. It goes down the back side of the ground plane to a manual switch which allows selection of two DC sources and passes through the ground plane near its bottom. From here, it progresses up the front side of the ground plane past the filter capacitors, crowbar ignitron, total current and trigger monitor, output selector switches, output surge resistors, output current and trigger monitors and output surge terminator networks to the three output terminals located below the front part of the ground terminal plate. All components are easily accessible for inspection or service.

The controls were all moved to their own control cabinet, completely outside and separate from the high voltage equipment cabinets. This not only provides electrical isolation for the sensitive

control circuits, but also allows personnel to work on the relatively safe control circuits without exposing them to the dangerous high voltage circuits. The crowbar electronics were reused with little change, having been redesigned by us in the past in attempts to overcome the false triggering and other problems which have plagued us from the beginning. All the interlock and control relay strings were re-designed from scratch in an attempt to simplify and complete the logic and to eliminate relay race problems which had caused problems in the past. The new relay circuits were built using modular techniques to reduce design effort and to simplify maintenance and future modification. Front panel displays were used extensively to indicate interlock failures and control logic status to make service quicker and more straight-forward.

The AC rectifier transformer, rectifier and filter choke were originally supplied in a single, oil filled tank located outside the building on a fenced-in transformer pad. Because of the difficulty in developing a transformer that would withstand the surge currents involved in this application, the oil in this tank (and thus the rectifier and choke) was frequently soiled with failed transformer debris. To protect the rectifier and choke, a separate tank was made for them some years ago, early in this 'development' process. The most recent design of the transformer seems to be much more robust than past designs, with coils of the stronger and more rigidly blockable disc configuration rather than the conventional (for this size of transformer) layer wound configuration of past designs. The failure-free performance of this unit has engendered such confidence that we have purchased a second transformer of similar design to be used as a spare. The spare transformer will be installed on the pad with high voltage cabling that will allow changing from one transformer to the other without moving them around and thus without having to remain shut down while awaiting the services of a crane.

The choke has also failed a couple of times since it was first supplied by Aydin, contaminating the rectifier and oil in the tank with choke debris. An analysis made recently of the electric and magnetic stresses on the choke, especially during load fault or crowbar conditions, resulted in a new design for the choke which would not fit in the existing rectifier/choke tank. Because of this, and the desire to make the rectifier and choke more readily serviceable (without the need for draining oil, etc.) it was decided to purchase a new choke and a new rectifier designed for operation in air in an indoor cabinet. This also provided space on the outdoor transformer pad for the spare transformer. A new cabinet (the Power Conversion Cabinet) is presently being built to house the choke, rectifier, and the step-start equipment. It will be installed indoors in the place previously occupied by the cabinet which held only the step-start equipment.

A quick description of the new Phoenix power system is as follows: Power at 13.2 kV comes from the building 13.2 kV bus to the Phoenix fused disconnect via a 15 kV class, 4/0 cable. The Phoenix fused disconnect feeds the Phoenix bus, which feeds the Phoenix vacuum contactor and its associated relaying. The Phoenix vacuum contactor feeds the step-start equipment, located in the new power conversion cabinet. The step-start circuit feeds the tap changer, which is located outside on the transformer pad, via a 15 kV class, 4/0 cable. The tap changer feeds one of the two rectifier transformers, also located on the transformer pad, which raises the voltage to 15.4 kV. The rectifier transformer feeds the rectifier, located in the new power conversion cabinet, via a 25 kV class, 2/0 cable. The rectifier output goes to the filter choke, also located in the new power conversion cabinet. The output of the choke goes from the power conversion cabinet to the DC distribution cabinet via R/G 220 coaxial cable. The DC distribution cabinet has three outputs, one for each RF amplifier.

As a final point of interest, since some of the work on the power conversion cabinet involved work on the 13.2 kV electrical system, the Michigan Department of Labor was contacted to find what codes and regulations were applicable. According to their Mr. Poke, the University is exempt from Michigan construction codes with few exceptions, those being where the State Fire Marshal has authority (residential or instructional buildings) and may require a permit. Although all work done on this project meets or exceeds the National Electric Code and other relevant codes, there are no permit or inspection requirements.

# Control Algorithm for the K1200 Cyclotron Main Magnet

A. McGilvra

The K1200 cyclotron main magnet is made up of two mutually coupled superconducting coils. The inductance of the coils is on the order of 100 henries. The coupling makes current control difficult because as the current in one coil is increased it tends to force the current in the other coil to decrease and vice versa. The coils are operated between 0 and 1000 amps depending on the magnetic field required. The currents must be held at their target values within about a milliamp. The control algorithm uses a modified form of neural network as an adaptive controller to accomplish this.

The first order model for the magnet is as follows:

$$Va = La * d(Ia)/dt + M * d(Ib)/dt$$
$$Vb = Lb * d(Ib)/dt + M * d(Ia)/dt$$

where:
- Va = Voltage applied to the 'a' coil
- Vb = Voltage applied to the 'b' coil
- Ia = Current in the 'a' coil
- Ib = Current in the 'b' coil
- La = Self inductance of the 'a' coil
- Lb = Self inductance of the 'b' coil
- M = Mutual inductance between 'a' and 'b' coils

The actual magnet deviates from this ideal model in that there is a small amount of resistance in the room-temperature leads that connect the power supply to the magnet. Also, the inductances change as the currents change because the magnet goes through saturation.

The control algorithm must deal with these non-idealities as well as with the problem of controlling an ideal magnet. The basic approach was to successively estimate the inductances and to calculate voltages from the model that will give the desired rates of change of the currents.

The first step is to calculate the desired rates of change or slopes:

$$Iadset = Iaerr / |Ierr| * gain$$
$$Ibdset = Iberr / |Ierr| * gain$$

where:
- Iadset = Set point of 'a' current slope
- Ibdset = Set point of 'b' current slope
- Iaerr = Difference between Ia and target Ia
- Iberr = Difference between Ib and target Ia
- $|Ierr|$ = Vector magnitude = $SQRT(Iaerr^2 + Iberr^2)$
- gain = Parameter that changes each iteration of the algorithm, explained below.

After the desired slope set points are calculated they are plugged into the magnet model above to calculate the voltages required to achieve the desired set points. These voltages are applied to the magnet coils by the magnet power supply. The magnet power supply has a maximum of 40 Volts on the 'a' and 'b' outputs. If the magnet power supply cannot achieve the voltages that are calculated then

'gain' is incrementally decreased for the next iteration. If the power supply does achieve the calculated voltages then 'gain' is increased.

The final step is to update the magnet model to keep up with changing inductances. This is done by treating the magnet model as a simple neural network with linear neurons and using the delta rule from the back-propagation method to update the inductances:

$$La = La' + LC * Iaderr / |Iderr| * Iadset / gain$$
$$Lb = Lb' + LC * Ibderr / |Iderr| * Ibdset / gain$$
$$M1 = M1' + LC * Iaderr / |Iderr| * Iadset / gain$$
$$M2 = M2' + LC * Ibderr / |Iderr| * Ibdset / gain$$
$$M = (M1 + M2) / 2$$

where: La', Lb', M1', M2' = Inductances from previous iteration
LC = Learning coefficient
Iaderr = Iadset - d(Ia)/dt
Ibderr = Ibdset - d(Ia)/dt
$|Iderr| = SQRT(Iaderr^2 + Ibderr^2)$

There are two mutual inductances (M1 and M2) because in a neural network they are two separate interconnect weights. However, since it is physically impossible for the magnet to have two mutual inductances the average of M1 and M2 is taken as the magnet's mutual inductance.

There are several changes in the algorithm made as the currents approach their targets: training (updating inductance values) is disabled to prevent truncation errors due to very small slope values; the method used to calculate 'gain' is altered to improve regulation; and the calculated voltages are integrated with a small integration constant to compensate for voltage dropped across the room-temperature leads and to improve regulation.

**Results**

The performance of this algorithm has been very encouraging. The regulation is well within the stability requirements of the cyclotron. The current path taken to get to the targets is generally straight and such that the two currents reach their respective targets at the same time. One exception to this is when the currents are being changed in such a way that no net energy is being put into or taken out of the magnet. Under these conditions the currents can change very rapidly which makes it difficult for the inductance calculations to keep up. When this happens the currents may significantly overshoot their targets but they always recover and regulate well.

# ELECTRONICS DOCUMENTATION

T.R. Jones and B. Palmer-Scott

The electronics department's documentation group has the following duties: creation and maintenance of the various drawings and publications produced and used by the department; technical writing; and printed circuit board design.

## Drawings and publications

Currently in our files, we maintain approximately 3500 drawings, artworks, and original films. We add to these files as the documentation is created for a particular project. Also, as changes to a current drawing become necessary, the files are updated. Along with newly created drawings, the documentation group keeps subscriptions to several computer and technical journals, a collection of hardback reference books, and current software manuals in the library.

## Technical writing

The process of technical writing and editing was systematized this year with the creation of a list detailing the steps in the writing/editing process, a documentation work order form, and a documentation evaluation form. These enables the writing/editing process to go more smoothly, in the following ways:

The *list of steps in editing* lets authors know what to expect, thereby avoiding dismay at what might appear to be an unduly lengthy process. The *documentation work order* lets the editor know what level of editing the author desires, from mere grammar and punctuation to sentence restructure; this understanding between author and editor avoids conflict. Lastly, the *documentation evaluation* measures the success of the process, and also reminds the editor what standard of performance is expected.

## Printed circuit boards

The documentation group also handles the design of the various printed circuit boards used throughout the electronics department. This is accomplished by using the OrCAD schematic capture and Protel circuit board software packages. We were using OrCAD printed circuit board software until the department changed over to Windows, at which time we converted to Protel. This was done ins a move to use a more advanced PCB software package, which in turn allows us to design better, more cost-effective boards.

The documentation group stores a wide variety of files in the computer for easy retrieval. These include AutoCAD, Protel, and OrCAD files used for the various applications. These are in turn backed up with a tape for secure storage. All of this is kept track by using Paradox database software.

A copy of each drawing is also kept on hand to make working copies from. These are kept in hanging and horizontal cabinets for protection.

One of the biggest areas the documentation group handles is the creation and maintenance of drawing "bundles." Originally, the bundles were blueprints of a particular system stapled together so that in the event of a failure, the technician could use this compiled information to repair the system in question. The fault with the arrangement was the bundles were easily damaged and lost. This last year we eliminated the staple blueprint style bundle in favor of yellow three-ring binders for each system, which holds all the information needed to perform service. This new bundle has proved to be a lot more durable and because of the color, harder to lose.

In conclusion, the documentation group has made several changes this last year to streamline the documentation process, create clearer, more usable work and make changes to existing drawings quicker. These changes benefit the electronics department and Lab in general by allowing the technicians to make necessary repairs faster, get new equipment into the field faster, and allow better tracking of current equipment.

# A CONTROL STATION BASED ON MICROSOFT WINDOWS

J. Vincent

A new variety of control console is being developed to be used in addition to some of the existing VAX workstations. This is being done primarily in response to NSCL needs, developments in industry, and partially due to changes in the NSCL computing environment. This console will be a primary focus of the controls group in 1992.

The console described will use Intel x86 ISA (Industry Standard Architecture) or EISA (Extended ISA) based computer platforms. The console will initially use the MS-DOS operating system (version 5.0 or later) and Microsoft Windows (version 3.1 or later). The software which interfaces this environment to the NSCL Control System (NCS) will be written in Turbo Pascal for Windows (TPW). The console may evolve into using the Microsoft NT operating system when it and suitable development tools become available.

The hardware and software were primarily chosen because of a) suitability to task, b) enormous installed base c) enormous base of manufacturers and suppliers leading to intense competition in price and support, d) enormous variety of inexpensive software and development tools, e) rapid development environment, and f) existing Electronics Department expertise. The rest of this paper will refer to this console as a WCS (Windows Control Station).

The WCS will communicate with the NCS (NSCL Control System) VME Stations via ArcNet using the so-called "classic protocol." One of the VME Stations will function as a data server to the WCS. (A "data server" is any standard VME Station which performs the function of gathering and distributing information to all other VME Stations on the network on behalf of a requesting station.) Using a data server relieves the WCS from the overhead and complexity of assembling list fragments from multiple VME Stations. A MS-DOS-based PC operating in the manner described is already in use at FNAL. FNAL uses a Token Ring network versus ArcNet.

The WCS will communicate with the NCS PLCs (Programmable Logic Controllers) via RS232 or ModBus Plus using the Modbus Protocol. The NCS currently uses Modicon-based PLCs exclusively.

The PLC and VME Station communication software introduced above will each be implemented as a MS Windows "Dynamic Link Library" (DLL). Both of these DLLs will interface to multiple clients simultaneously in a similar fashion. Incoming data will be available as either regularly polled buffered lists or as one-shot requests. Outgoing data will be one-shot lists of settings or as a one-shot individual setting. Incoming broadcasts will be separately buffered from incoming addressed data. Data will be transferred to client processes from the server (DLL) process through shared global memory.

The server allocates and de-allocates memory on behalf of each client. The memory, which is owned by the client process, is allocated as non-movable to prevent delays in server operations. The memory returns to the system should the client be terminated for any reason. Although the data

addresses are fixed in memory, the server shall request a pointer to the memory from the system prior to each use to ensure the memory is still valid. If the memory is invalid, then the client has terminated and all server processes for the client are gracefully terminated.

The method of communicating to the control system described using DLLs will result in allowing any MS Windows-based compiler or development system to develop controls applications. The controls group will develop (on a need and priority bases) procedural (and in some cases object-oriented) bindings to suitable development systems. The initial procedural bindings will be for MS FORTRAN and TPW, and the initial object-oriented binding for TPW. Standard applications developed by the controls group will consist of applications like knob controls, meter controls, multichannel displays, alarm servers, chart recorders, push buttons, probe controls, beam pot controls, target ladder controls, ECR charge state plots, logging programs, setup programs, etc. Whenever possible the programs will be developed as MDI (Multiple Document Interface) applications. Multiple instances of programs when the process is non-exclusive will also be possible. The controls group will encourage and assist in training responsible individuals in writing their own applications.

In conclusion, a control console based on MS Windows and Intel x86 based computers will be developed. Development hardware and software for this project is already available. It is projected to take approximately 90 days to get the base system operational. Applications will then be written on a priority basis.

# INTEGRATING THE K500 CONTROL SYSTEM INTO THE NSCL CONTROL SYSTEM

J. Vincent, L. Foth, and J. Priller

## I. Introduction

This report summarizes the integration of the K500 controls into the NSCL Control System (NCS). The integration is complete at the time of this writing. The four types of controllers which are now integrated into the NCS are: the PSC (power supply controller); the BBSP (bang-bang servo with potentiometer feedback); the BBSE (bang-bang servo with incremental encoder feedback); and the BCM (beam current meter). The devices controlled by the K5CS that were affected are:

1) 18 cyclotron trim coil power supplies (18 PSCs)
2) 2 cyclotron extraction system electrostatic deflector high voltage power supplies (2 PSCs)
3) 2 cyclotron beam probe drives (2 BBSEs)
4) 2 cyclotron beam slit drives (2 BBSPs)
5) 14 cyclotron extraction element drives (14 BBSPs)
6) 6 cyclotron dee stem drives (6 BBSEs)
7) 8 beamline slit drives (8 BBSPs)
8) 7 cyclotron beam probe beam currents (7 BCMs)
9) 14 extraction element beam currents (14 BCMs)
10) 11 beamline beam currents (11 BCMs)

The remainder of this paper is a technical overview of the system and the process of integrating it into the NCS. Particular attention is given to the cyclotron beam probes and electrostatic deflectors due to their operational complexity. For a complete technical description of this system see NSCL Electronics Department manual Integrating K500 Control System Devices into the NSCL Control System.

## II. Overview

The K500 Control System (K5CS) is based on CAMAC, the AP (auto-polling) bus, and, prior to this upgrade, a PDP 11/34 computer. Connecting CAMAC to an AP bus is the APT (auto-polling transceiver) module, which translates appropriate CAMAC messages into AP bus messages. The APT module consists of 32 memory cells: 16 read and 16 write. CAMAC functions allow one to write one set of 16 and read the other set of 16 cells. The auto-polling transceiver updates the CAMAC registers with the data acquired from the devices every 60th of a second. It triggers "writes" to the devices when new data is available. On the user end, an AP bus is used to connect boxes containing knobs, buttons, multiplexers, switches and meters to CAMAC. (Knobs, etc., are all on the console in the Control Room,

away from the devices they control.) At the device end, an AP bus is used to connect power supply controllers (PSC), general-purpose I/O (GPIO), and bang-bang servos (BBS) to CAMAC. The only other device in this system is the beam current monitor (BCM), which connects to CAMAC directly.

A PDP 11/34 computer performed data acquisition and distribution to all the devices through this CAMAC system. In addition, a program which ran on the 11/34 created the logical connections and functionality between the user interface controls (knobs, meters, etc.) and the devices being controlled (PSC, BBS, etc.) The 11/34 was booted and maintained by a VAX 11/750 through 1 port of a 4 port shared memory module. This same port allowed the 11/750 to monitor all of the control parameters in the 11/34. Another port of the shared memory module was attached to a VME station which was used to acquire K500 cyclotron beam probe data from the 11/34. *See Figure 1.* The beam probe data was then used by VAX stations to generate data plots of cyclotron internal beam versus radius.

Because the 11/750 will be removed as a result of the NSCL computer system upgrade, the 11/34 would loose its boot mechanism. Therefore we decided to integrate the K500 devices into the VME-, ArcNet-, EtherNet-, and workstation-based NSCL Control System (NCS). Since the NCS already handled user-interface controls (via local consoles and workstations), the K5CS user interface controls were eliminated.

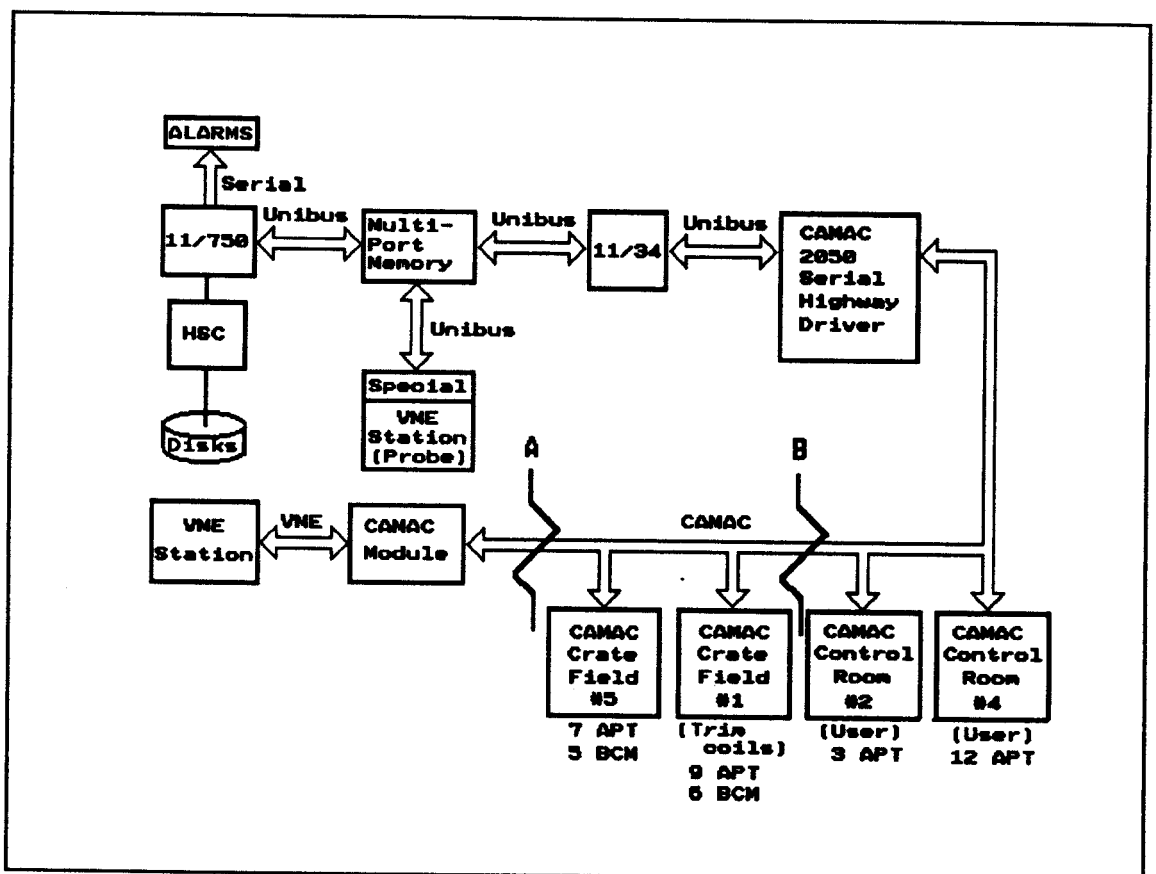


**Figure 1**: Past configuration and redesign of K500 control system. Everything to the right of and above point 'B' was functionally replaced with the CAMAC module and VME station to the left of point 'A.'

This manner of maintaining the link to K5CS devices was the least costly and manpower-intensive of the options studied. The linkage was accomplished by a VME-to-CAMAC module and CAMAC crate controllers. These modules are identical to the units used on the NSCL data acquisition system.

## III. Items That Were Reconfigured

After evaluation of the intended use, function, and history of the devices on the K5CS, it was determined that a few devices should be removed from this system and integrated directly into the NCS when needed. The devices removed were six servos which activated the K500 dee stem drives and two deflector high-voltage controllers:

### 1. Dee Stem Servo Controls

The dee stem servo controls always had a problem maintaining calibration and were never very reliable. These controls should not have been in any remote control system in any case, because it was only legitimate to actuate them from the K500 RF control balcony. They were replaced with less complicated servo controls which are based on technology developed for the K1200.

### 2. Deflector High-Voltage Controllers

The deflector high-voltage controllers had been specially modified, which made them difficult to maintain. Since special inexpensive buffer amplifiers were developed for the K1200 deflectors and ECR anyway, we elected to use them instead. NCS control system channels already existed to control these devices.

## IV. Cyclotron Probes and Electrostatic Deflectors

The old K500 control system for the probes and deflectors used servo "counts" when reading and positioning servo motors, and 100th-inches in calculating and reporting radii. These units have been retained wherever possible in the new NCS-based control system code, and are the units used in configuration file entries unless otherwise noted.

To obtain servo counts from the VME stations, the scaling factors for each servo are read in and used to "reverse" the scaling into a 0..4095 count range (or 0..65535 in the case of the main probe).

### K500 Main Probe

The main probe on the K500 cyclotron follows a curved track, unlike the other K500 and K1200 probes that move along a straight line. Servo positions are determined via a look-up table of servo position-to-cyclotron radii values. The probe is positioned by sending servo positions to NSC channel 5MPRB. In the current control system, the look-up table is stored in the file K500MP_TABLE. Running the probe can also be accomplished through "run-plus" and "run-minus" bits in the channel 5MRUN.

**Configuration:**

The configuration file for the K500 main probe is 5M_PROBE_CFG.

**Calibration:**

The scaling constants in the VME stations are set up so that the reading of the probe position channel (5MPRB) is correct in two locations: when the probe is fully extended, and when it is fully retracted (2.04 and 51.24 inches, respectively). If recalibration of the probe becomes necessary because of some change in geometry, measurements will have to be taken within the cavity for these two locations and the scaling constants changed. For simple software calibration, the probe is run out to its fully retracted position, the correct position value (51.24) is sent to its calibration channel (5MCAL), and the calibrate bit of this channel pulsed.

**K500 Viewer Probe**

The viewer probe for the K500 follows a straight path along a radius line from the center of the cyclotron, and therefore requires no special software scaling or other calculations to determine its position. This is all handled in the VME stations, where the current radius position may be read and set directly from the control channel, 5VPRB. Running the probe can also be accomplished through "run-plus" and "run-minus" bits in the channel 5VRUN.

**Configuration:**

The configuration file for the K500 viewer probe is 5V_PROBE_CFG.

**Calibration procedures:**

If changes in geometry have taken place, measurements of the fully extended and retracted positions will need to be taken (they are 17.84 and 30.63 inches for the current probe) and the scaling factors of the 5VPRB channel changed to reflect this. Otherwise, the probe is run out to its fully retracted position, the correct value (30.63) written to the calibration channel (5VCAL), and the calibrate bit of this channel pulsed. If a different probe is installed (one other exists), new measurements will need to be taken and those values used for calibration.

**K500 E1 and E2 Deflectors**

Each of the two K500 deflectors, E1 and E2, has a peculiar "teeter-totter" geometry that makes direct user control of their servo motors somewhat difficult. As the deflectors do not possess sufficiently safe hardware limiting, direct user control of the servos is unsafe as well. For these reasons a detached process on a MicroVAX workstation is used to monitor user-requested settings for deflector radii (channels K5E1E and K5E1X for E1, K5E2E and K5E2X for E2), and handles moving the servos in a safe fashion. These channels appear to the

user as the actual deflector radii, all servo maneuvering and safety precautions go on within the VAX process, transparent to the user. A Modicon enable bit is used to prevent the servos from being moved by users or other processes. The monitoring program (and a cooperating process on a VME station) also handle "mirroring" the calculated deflector radii and servo status bits to the user's radii channels.

**Configuration:**

The configuration file for the K500 deflectors is K500_DEFLECTORS_CFG.

**Calibration procedures:**

Calibrations necessitate taking new measurements within the K500 cyclotron and deriving new deflector equation coefficients. This is done by taking numerous measurements for different values of SI and SO, and deriving the coefficients using a regressive fit.

## V. Available Test Equipment (* denotes built as a result of this project)

1. Two AP Bus Simulator Modules
2. AP Internal Bus Simulator*
3. CAMAC Module Tester Bi Ra Model 6103
4. AP Module Simulator 64
5. PSC Voltage Test Box
6. APLC Test Fixture
7. AP Bus Address Selector*
8. Auto Polling BCM PA Tester*
9. IBM-PC with CAMAC link and test software (in Nuclear Electronics Dept.)

## VI. Test Software

Some PC-to-CAMAC test programs have been developed to help the electronics shop repair and maintain the K5CS devices. This software was written in Pascal for the PC-to-CAMAC link that nuclear electronics has for testing modules. The collaboration between departments paid off, for nuclear electronics has also received a test program and an easy-to-use programming environment for the PC-to-CAMAC link. This is valuable because the current software runs on the "test" VAX due for removal also.

The source code was written (as much as possible) to conform to IEEE standard 758-1979, which defines how FORTRAN-"call"able CAMAC subroutines should look and function. We applied this CAMAC standard to the hardware we're using (i.e. PC-to-CAMAC board, crate controller, and PC

platform.) Although the standard was designed with Fortran in mind, it was easily written in Pascal. This code formed the basis for an object hierarchy which was used to develop the user programs.

## VII. Conclusion

The K500 Control System has been successfully integrated into the NSCL Control System. The project went smoothly with few unexpected occurrences. The authors thank the NSCL Computer Department for their courteous assistance in gathering information and assisting with some of the system's idiosyncracies. Hopefully the system will now be more easily operable and maintainable.

# RF PHASE SELECTION IN THE K1200 CYCLOTRON

J. Bailey, F. Marti, J. Kuchar, J. Yurkon, J. Nolen, and K. Kranz

Phase Slits, similar to those installed in the K500[1], have been installed in the K1200. A silicon detector intercepting an attenuated beam is used to measure the time structure of the extracted beam. Reductions to 4° of RF phase width have been achieved to date. Beam losses from the slits have been minimized to 70% while cutting to 5°.

The design of the K500 phase slits has been ported over to the K1200. The shaft, bellows, and pin needed lengthening, and a new base was designed to mount the drive on the K1200. Two major changes were the mounting of a Bimba air cylinder on axis for insertion, and the replacement of the rotation drive cables with a drive shaft. The rotation is driven with a Slow-Syn motor mounted 8 ft. above the cap, and shielded with 1/2 in. cold rolled steel. An Ultrasonic motor was investigated for use in the magnetic field. Its phase shifting circuitry (mounted on the Mezzanine East wall) still required shielding. Rapid smoothing of its friction surface reduced the applied torque, causing repeated failures of the drive. Panasonic removed them from the market for similar problems, so we used the Slow-Syn.

A silicon detector, intercepting a greatly attenuated beam, has permitted rapid measurement of the extracted beam time structure. This would not be possible without the use of attenuators of the order of $10^{-6}$ in the injection beam line. (Nor would it be useful if beam intensities were large enough for space charge effects.) We amplify the signal from an LBL Time Pick-Offs, process it in a constant fraction discriminators, then use it as a start signal. The stop signal is taken from the RF, and the digitization of the time difference is done in a CAMAC crate connected to a VAX computer on the serial highway. A time resolution of 340 ps FWHM was measured with 40 MeV/A alpha particles transmitted through two detectors. These leave $\sim$ 1 MeV in each detector.

Table 1 shows some data obtained in the first few uses of the slits. Figure 2. shows how the cut beam's time structure drifted and fluctuated in a 7 hr period. The cyclotron controls and the phase slits were not touched. The only change in the control readings, was a change in the outer yoke temperature of +.2° C. It is not known what caused the drift, but the net change is 2 parts in $10^5$ of the $\sim$ 800 turns inside the K1200. The uncut beam was found to have drifted the same net amount at the end of the measurement. All of this demonstrates a need to monitor this time structure, after tuning the phase slits. A program is being written that will display and store old and new spectrum for comparison, to aid the

Table 1: Phase cuts and transmission.

| Ion | Energy (MeV/A) | $\phi_{FWHM}$ uncut | $\phi_{FWHM}$ cut | $I_{cut}/I_0$ |
|---|---|---|---|---|
| $^{17}O^{3+}$ | 25 | 15.°RF | 5.7°RF | .33 |
| $^{16}O^{5+}$ | 50 | 12.7°RF | 7.8°RF | .24 |
| $^{24}Mg^{7+}$ | 60 | 11.°RF | 2.6°RF | .25 |
| $^{18}O^{6+}$ | 80 | 14.5°RF | 4.7°RF | .30 |
| $^{28}Si^{9+}$ | 80 | 12.°RF | 4.6°RF | .23 |

operators in this process.

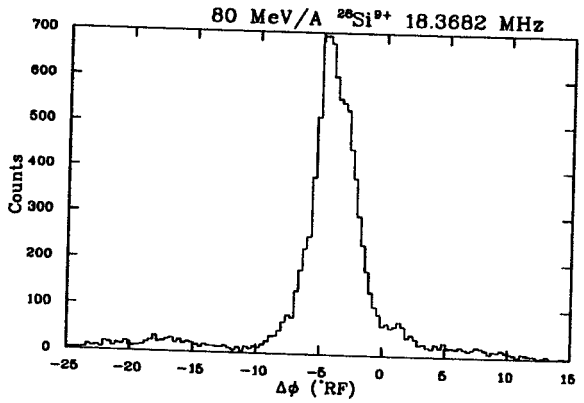


Figure 1: The best extracted beam phase width to date. The FWHM is 3.6° RF, or .55 ns at this frequency. Lower widths in the main peak have been achieved, but with larger shoulders and satellites.

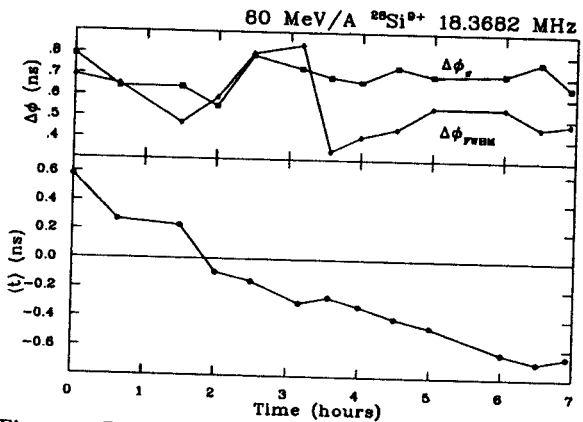


Figure 2: Tracking, over time, of the extracted beam time structure transmitted through the phase slits. Presented are the first and second moments, and the FWHM of the main peak. The cyclotron was not retuned during this time. The centroid drifted, and the structure fluctuated.

Currently an internal timing probe is under construction. Interchangeable with the camera probe, it should allow us to separate the effects of the slits from those of extraction. We also will measure the phase history of the beam. Together, the two probes will aid in studying beam dynamics near extraction.

## References

1. Milton, B., "Phase Selection in the K500 Cyclotron and the Development of a Non-Linear Transfer Matrix Program," Ph. D. Thesis, Michigan State University, 1986.

# PC RESON: RADIO FREQUENCY CIRCUIT ANALYSIS FOR PC'S

J. Vincent and J. Priller

RESON is an enhanced AC circuit-analysis program modeled loosely on Spice. The program has been used in the analysis and design of the K1200 transmitters, resonators, bunchers, Harper Cyclotron, etc. "Enhanced" means that beyond solving for voltages and currents, RESON computes circulating and dissipated energy, and allows for material properties and geometry. RESON also has additional output functions and formats.

All of RESON's input and output files are standard ASCII. Input files look similar to SPICE input files. Input files contain statements and comments which describe the circuit and the analysis to be performed. Output files have quote-delimited strings and comma-delimited numeric fields, so that they may be easily imported into spreadsheets or scientific plotting programs.

RESON requires the MS-DOS or PC-DOS (version 2.1 or higher) operating system. It also requires an x86 IBM-compatible PC, and 640k of ram. A math co-processor and hard disk are recommended but not required.

The circuit that RESON is to analyze is described in a ASCII file by a netlist. A netlist is a group of statements, each of which identifies a circuit element, its interconnecting nodes, and its properties. In addition to the netlist, a RESON input file contains commands that direct the analysis to be performed and the output(s) to be generated. An input file may also include comment lines, which typically described the circuit and analysis for future reference.

RESON's AC analysis solves for the small-signal frequency response. All non-linear elements are made linear about the operating point by user input model parameters. For example, if the model parameters specify a gain of ten, then the gain remains ten no matter what the input level.

RESON computes and returns output based on user-specified parameters in the .OUTPUT and .PRINT commands. The following output functions are available.

1. V (node voltage)
2. VT (element terminal voltage)
3. I (current through a voltage source)
4. IT (current into a device terminal)
5. IS (current into a node from all attached current sources)
6. IN (the total current entering a node)
7. Pc (the total conduction losses in the specified circuit element)
8. Pe (the total losses due to electric fields in the specified circuit element)
9. Ph (the total losses due to magnetic fields in the specified circuit element )
10. Ue (the total electric energy stored in the specified circuit element)
11. Uh (the total magnetic energy stored in the specified circuit element)
12. Q (the quality factor of the specified circuit element)
13. N (the node number that the specified circuit element's terminal is attached to)

RESON's element statements describe the circuit that is to be analyzed by a netlist. The following circuit elements are available.

1. C (capacitor)
2. K (coupled coil)
3. L (inductor)
4. R (resistor)
5. V (independent voltage source)
6. H (current-controlled voltage source)
7. E (voltage-controlled voltage source)
8. I (independent current source)
9. F (current-controlled current source)
10. G (voltage-controlled current source )
11. T (general transmission line)
12. TC (coaxial transmission line)
13. TR (rectangular transmission line)
14. Y (tetrode vacuum tube)
15. O (operational amplifier)
16. Q (BJT [bipolar junction transistor])
17. J (FET [field effect transistor])

In conclusion, RESON is a very flexible and powerful program useful for any type of AC circuit analysis, in particular RF circuits. It can solve circuits of over 100 nodes on any IBM-compatible PC with 640k of ram. RESON is available from NSCL, Compuserve (IBM Applications forum), or from some mail order shareware vendors.

# S800 PROGRESS REPORT

A.Zeller, S.Bricker, R. Swanson, J.DeKamp, B.Zhang, J.Nolen, B.Sherrill, H.Blosser, M.Berz, H.Laumer, R.Fontus, T.Jones, A.McGilvra, E. Kashy, D. Pendell, L.Morris, H.Hilbert, D.Lawton, C.Snow, C.Magsig, and D.Sanderson

The supplemental funding from the NSF for completion of one of the two S800 dipoles has allowed us to concentrate on construction of the dipole and testing of parts which are needed for both dipoles. We have attempted to secure parts for both dipoles whenever possible, within the budgetary constraints. Upon the submission of the proposal to the NSF for funding to complete the whole S800 project, we have changed the direction of our assembly sequence to enhance the timescale for S800 completion. This mainly involved a decision to assemble the dipole on the carriage in the pit. This allows us to use our in-house crane capacity for assembly and does not require extensive rearrangement of the East High Bay. Additionally, it means that we will not have to disassemble the dipole after it has been mapped so that it could be placed on the carriage at a later stage. The status of various parts is given below.

## Coil Winding

As anticipated, it took considerable effort to develop a winding technique that allows us to wind the negative curvature side of the dipole. Each turn must be placed in its own slot in the G10 insulation pieces (12.5 turns per layer and 28 layers) and other G10 pieces used to allow turn-to-turn and layer-to-layer climbs to be used. The solution involves the use of many clamps which hold the wire in place on the negative curvature side. These clamps are alternately unclamped and clamped as the winding arm goes by. This is shown in Figure 1. A maximum winding rate of one layer per day is possible, while the normal rate is four layers per week. One of the two coils has been wound and sealed into the bobbin. Winding of the second coil is in progress.

## Cryostat construction

A cryostat has been designed which allows the magnet to be assembled vertically and which minimizes the amount of turning about of the pole tip assembly. Partial assembly can be done on the bench using the iron yoke and pole tips as assembly fixtures, then the bobbin is inserted with the nitrogen shield partially assembled. The final assembly and closure is done in the vertical position on the yoke steel. After complete assembly, the lead structure and helium dewar will be attached. To ensure that the coil is completely immersed in liquid helium, the liquid is brought into a dewar, which also contains the leads, and is phase separated. High quality liquid is then delivered to the

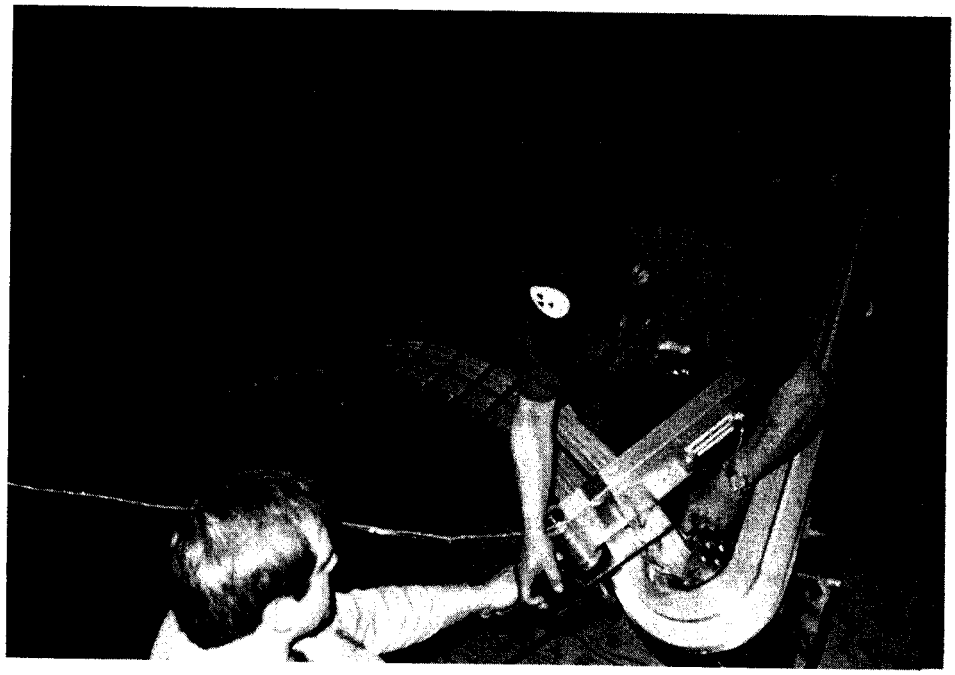

Fig 1 Winding the negative curvature side of the dipole.

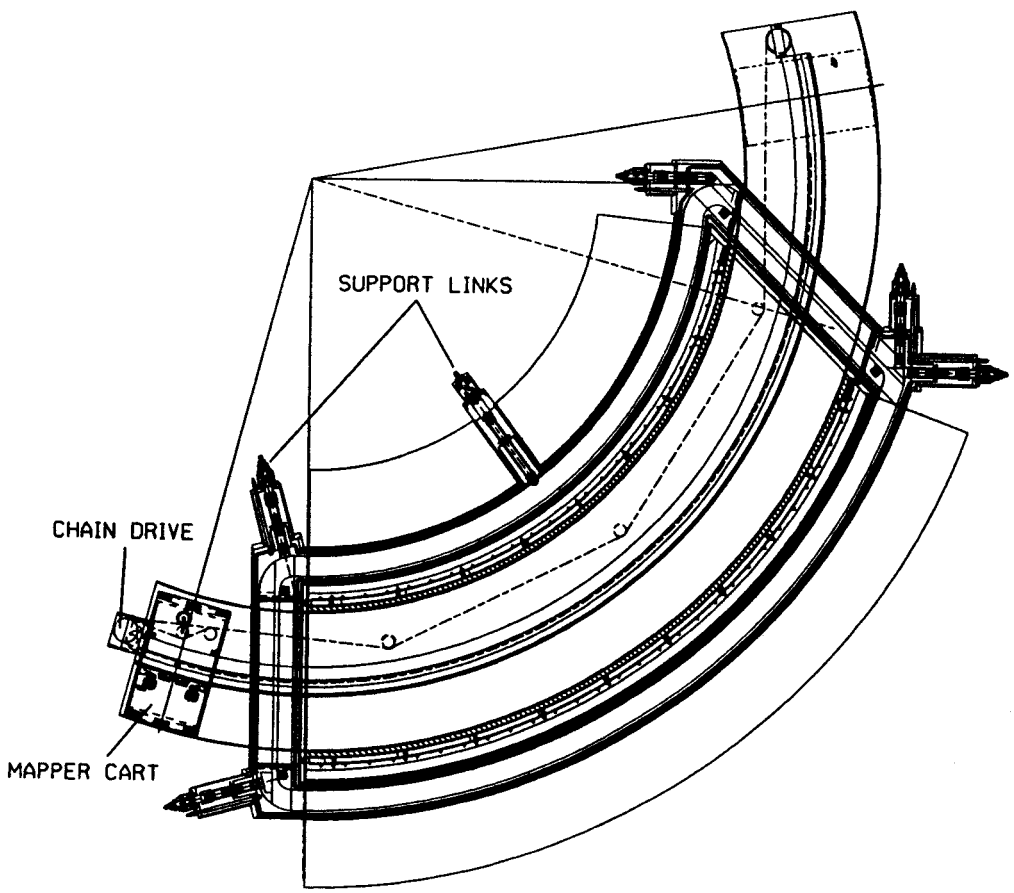


Fig 2 The dipole mapping apparatus.

bottom of the coil. All wire splices were made near the top of the magnet to ensure that they are still covered by liquid, but that any bubbles formed will not have to move up the coil to the leads. Numerous slots in the insulation also ensure that bubbles will not be trapped someplace in the coil package.

**Mapping apparatus**

The mapping apparatus has been designed to allow the use of five search coils, from below the median plane to well above it. This allows us to measure the field, and the derivative of the field, off the median plane. This is very useful for the ray reconstruction at the focal plane[1]. The position of the mapper cart along the circumference will be measured by an optical sensor which will see small slots laser cut into a stainless steel strip every 1mm. The radial changes will be made outside of the magnet. This allows us to map a magnet in about twenty hours. Figure 2 shows the mapping apparatus.

**Quadrupole design**

Design for the two quadrupole between the target and the dipoles (Q1 and Q2) has continued. Two dimensional magnets have been designed, including conductor specifications. The complete design will be confirmed with three dimensional calculations to determine the effective lengths. The ends of the quadrupoles will be bevelled. The present design uses the effective lengths based on a very similar design used at CEBAF[2]. Additionally, a sextupole winding for Q2 has been designed. This quad operates at low saturation, hence the Cos $3\theta$ sextupole, used to reduce the $x/\theta^2$ aberration, is a very good sextupole despite the quadrupole symmetry of the iron. The sextupole windings will be wound on the surface of the helium containment bore.

**Status**

The trim coil winding fixtures are being machined and trim coils will soon be wound. Design of the carriage continues. The yoke pieces will presently be sent out to have the lifting fixture and support bracket holes drilled. We hope to have the dipole ready for testing by the end of the year.

References

1. M. Berz, et al., MSU Ann. Report 1990, 242.
2. Conceptual Design Report CEBAF Basic Experimental Equipment, April 13, 1990.

# S800 BEAMLINE QUADRUPOLE AND DIPOLE CONSTRUCTION

C. Magsig, J. DeKamp, and A. Zeller

The beamline for the S800 Spectrograph consists of five superconducting quadrupole triplet magnets and four superconducting dipole magnets. In addition to acting as a high resolution beam preparation line for the S800, the line can be used as another A1200 fragment separator. Instead of two horizontal 45 degree bends as in the A1200, the beam must be transferred from grade level to the pit floor with two vertical bends. Because of the unusual location of the spectrograph, the beamline is mechanically more complex than normal. Three quadrupole triplets are horizontal but two quadrupole triplets are mounted at a 45 degree angle. The dipole magnets are also situated differently with two mounted vertically at a 22.5 degree angle and two mounted vertically at a 45 degree angle. The beamline is shown in Figure 1.

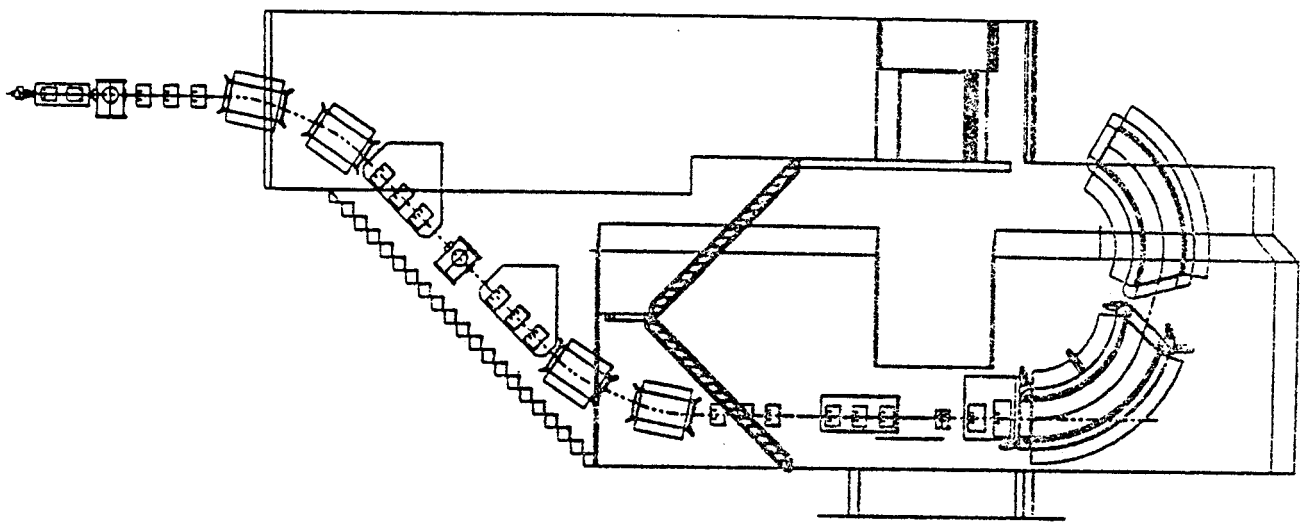

Figure 1

## Superconducting Quadrupole Triplet Construction

The quadrupole triplets are designed with a larger 20.3 cm aperature compared with the beam transport quadrupoles which have a 12.7 cm bore, as shown in Figure 2. The larger aperature quad develops a maximum gradient of 28 T/m generated by a maximum operating current of 43 amps. The coils

are wound with about 3400 turns of 0.5 mm diameter wire. Pricing considerations for machining of the magnet steel assemblies resulted in purchasing the steel and machining the assemblies in house. The steel to machine the yoke and pole tips is now in house and fixtures are being made to perform the required machining. A machine shop lathe is being upgraded to hold tighter tolerances required for the magnet. Coil winding forms were machined in house and preliminary winding of the coils has begun. They will be wet wound with a filled epoxy using our semi-automatic winding table. We now have enough of the superconducting wire for the quadrupole coils to wind two coils for testing. Design of the cryostats are universal so that the magnets can be placed either at a 45 degree angle or horizontal. Other components we have taken delivery of include valves, pressure transducers, pop-offs, bellows, and flowmeters.

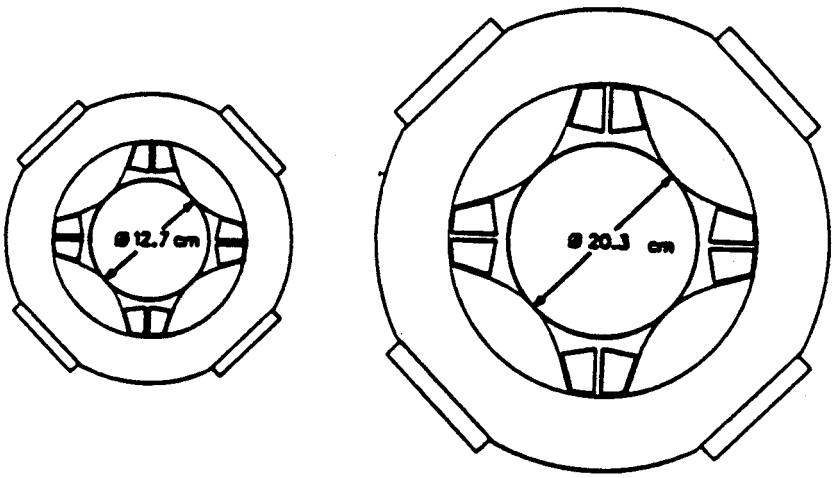


Figure 2

## Superconducting Dipole Construction

The S800 beamline requires that dipoles bend in the vertical plane relative to the conventional beam transport system. As a result the dipole steel is rotated and then tilted to its respective angle. The dipole steel and cryostats were also designed for univeral applications. The dipole steel was machined by an outside fabricator and is in house. The dipole bobbins were also machined outside and are ready for welding. The wire for the coils is in house and winding will start soon. The dipole coils are identical to the existing 22.5 degree dipoles which consists of 0.6 mm diameter wire, wet wound 600 turns with a filled epoxy. The peak field is 1.75 T while operating at 91 amps. The upper cryostat details are being finalized and will be sent out for bid soon.

# S800 SPECTROGRAPH DIPOLES COIL BOBBIN SUPPORT

J.C. DeKamp, R.T. Swanson, and A.F. Zeller

The coil bobbin support system for both of the S800 spectrograph's superconducting dipoles have been designed. Complete bobbin analysis has been done to determine the best link placement and provide links of proper strength. Sample support links were fabricated and tested, followed by a refined analysis. All of the links needed for both dipoles, two tubular fiberglass compression links and 54 fiberglass loop straps for the 27 tension links have been fabricated. Final link testing on completed link assemblies including hardware is in progress. The link heat load contributions are 0.85 W at 4K and 6 W at 77K for each dipole. A detailed description of the S800 spectrograph has been given elsewhere[1-4].

## Bobbin Analysis

Finite element analysis of the bobbins was done to determine link placement and find loads needed to properly resist the gravity and magnetic forces, as well as to provide adjustability after cooldown. Loadings at high field when the steel reaches magnetic saturation were determined[2] from a 3D magnetostatics analysis using TOSCA. The forces at the ends were over estimated for calculations at 1.7 T as they increase quickly with saturation. At the nominal operating field of 1.5 T, saturation is greatly reduced and the end forces are much smaller. Additional calculations were done at one half of the loading of the 3D results with no end forces simulating the point where end saturation begins to occur. The high force calculations thus include a good safety margin over expected operating conditions at 1.5 T. Bobbin analysis for magnetic loads perpendicular to the median plane was not done since for centered coils the loads are smaller, and the bobbin is 10 times stiffer in this direction vis-a-vis loadings parallel to the median plane. The initial analysis for only magnetic loads parallel to the median plane showed that the bobbin had larger displacements than wanted when freely deforming under the maximum load condition (1.7 T). These displacements were over 12 mm (.48 in) as shown in Figure 1. Clearances between the bobbins and LN2 cooled shields are only 12.7 mm (0.5 in). This leaves almost no clearance for operation which may already be reduced by assembly tolerances and necessary adjustments. Reducing this deformation could only be accomplished by stiffening the bobbin structure or by using additional support links. Support links were chosen since enough stiffening could not be added in the allowable space. This stiffening also would have had to be welded, creating distortion which would be hard to remove. Support links were then added to the analysis to decide on the best link configuration and size.

## Support Geometry And Link Forces

The first dipole bobbin with its chosen support configuration is shown in Figure 2. The dashed lines show its position at zero field, after cooldown and support preloads. The loads and total displacements for the nominal loading is shown in Figure 3, and for the maximum loading in Figure 4. The bobbin displacements are restrained with the help of the compression link on the inside curvature and two tension links at the corners of the outside curvature. These links reduced the spreading of the curved sides by over a factor of two (7.9 mm vs. 19.1 mm). The compression link was easy to add to the design because of a hole already machined into the yoke side which was originally envisioned to provide for a tension link to carry the unbalanced magnetic loads. The unbalanced magnetic loads are now carried by the tension links at the corners of the inside curvature. Another tension link is present at the upper corner of the outside curvature to help support the bobbin gravity loads and provide for adjustment after cooldown. This link is preloaded so it will not go into compression when the field is on. The links at that corner were purposely oriented horizontally and vertically to give a natural adjustment reference at one corner. The displacements on the ends are almost entirely due to the thermal effects while the ones on the curved sides are due to the magnetic loading which causes deformations larger than those needed to counteract the thermal component. Fewer links could have been used but some would have had to operate under both tension and compression. This could create some instability when loads are close to zero so this option was rejected. The second dipole bobbin link configuration is similar and is shown in Figure 5. Another tension link was added to the second dipole because of its different orientation with respect to gravity. The extra tension link added to the design for the first dipole is still needed for adjustability, with the other links still providing their function of restraining deformation and resisting magnetic loads. Small adjustments were made in some link directions to provide for clearence in critical areas and to give a natural adjustment reference.

There are 8 tension link assemblies which restrain each bobbin on the median plane, two opposite each other at each corner. These links are sized to safely handle unbalanced loads of 45kN (10 kips) per link due to coil displacements off the median plane.

## Bobbin Stresses

Restraining the deformations of the long curved portions of the bobbin together with the very stiff corners and ends which also have a stiffer section places the highest stresses where the long curved sections and corners meet. The highest stresses occur on the outside curves at the 90 degree corners. For the maximum condition this stress is about 345 MPa (50 ksi). The nominal operating

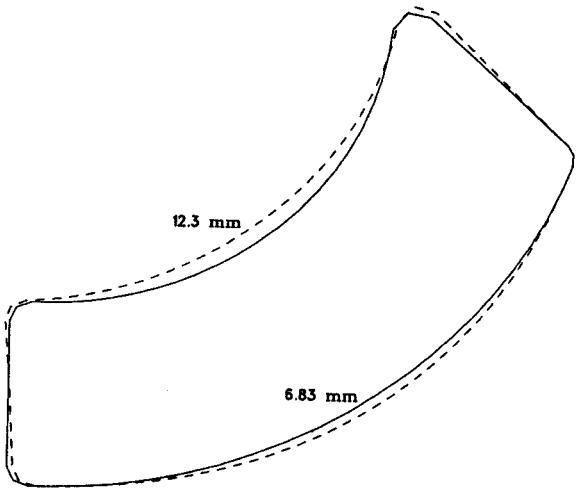


Figure 1: Displaced shape of bobbin deforming freely under coil forces at a field of 1.7 T in the 15 cm gap.

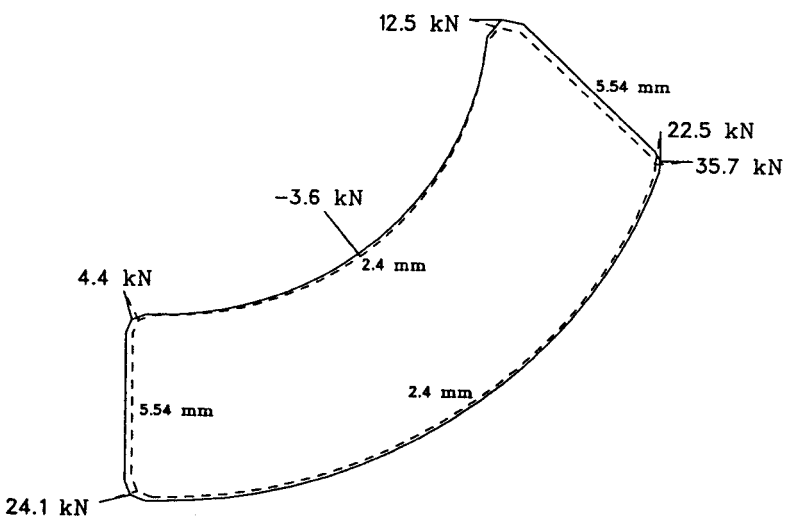


Figure 2: First dipole bobbin after cooldown and link preloads, at zero field. Its initial operating position is shown by the dashed lines.

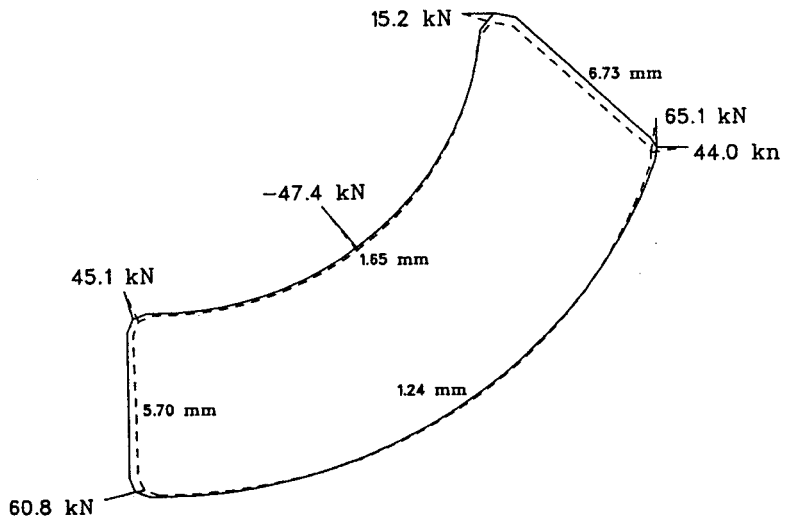


Figure 3: Support link forces and displacements for the first dipole bobbin at the nominal field of 1.5 T.

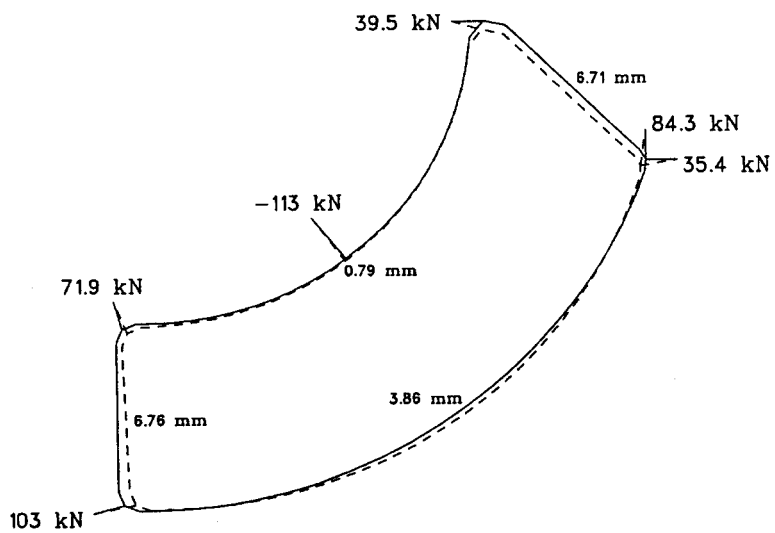


Figure 4: Support link forces and displacements for the first dipole bobbin at 1.7 T.

stress is 166 MPa (24 ksi). The bobbin material is annealed 316 S.St. with a yield stress of 207-241 MPa (30-35 ksi) at ambient temperature but increases to over 552 MPa (80 ksi) at 4K.

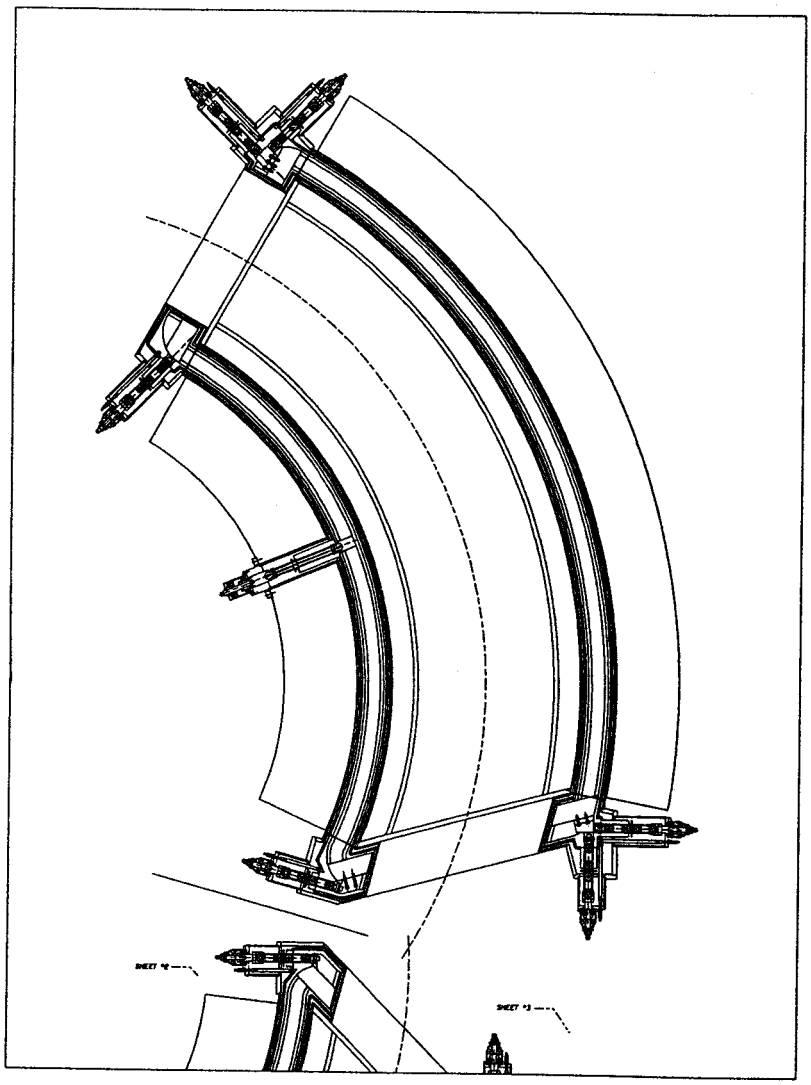

Figure 5: The support configuration for the second dipole.

## Support Link Fabrication And Testing

Sample links and hardware were constructed and tested at room temperature to determine final link sizes and hardware design. The actual links have all been fabricated. The tension links are fabricated from Scotchply SP-250-S29 "S" glass unidirectional prepreg tape wrapped around 304 S.St. bushings to form a looped strap. They were then oven cured. This type of link has been used successfully on other devices at the NSCL (eg, the Harper cyclotron and the superconducting ECR). The median plane restraint links use 20 layers of the .008" thick tape and the links parallel to the

median plane use 28 layers. The heavier links also are wrapped around larger bushings. The breaking strengths of these links are 156 kN (35 kips) and over 222 kN (50 kips) respectively. Since the link strength increases when cold, the cold end links could be made smaller if wanted. This was not done since the heat loads are clearly small and any link breakage should be at the warm end where link replacement is easiest. The links utilize titanium (6Al 4V ELI) hardware whose high strength is needed because of limited space.

The compression links were fabricated using Randolite PD43 fiberglass tubing epoxied to Ti hardware. A small Ti rod runs through the middle in case of epoxy joint failure which could allow the link to separate during assembly and cooldown. This rod can also carry some tension load if accidentally applied. The estimated compressive strength of this link is 356 kN (80 kips) and has been tested to 200 kN (45 kips).

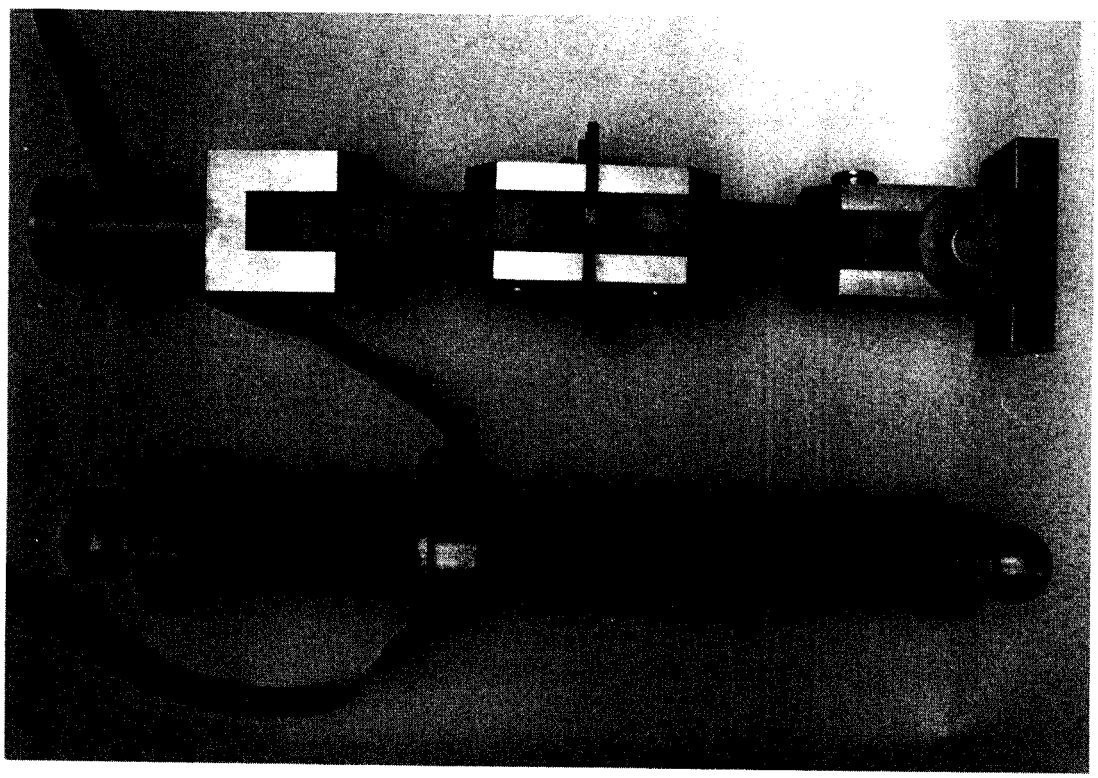

Figure 6: Tension and compression link assemblies. The tension link is on the top; the compression link is on the bottom.

Final testing of entire link assemblies will be done to determine actual warm and cold properties. Tension link and compression link assemblies are shown in Figure 6. Proof loading of all links will be done to insure against defects.

References

1. A.F. Zeller et al., "Construction of a Large Superconducting Spectrometer Dipole Magnet with Negative Curvature", Advances in Cryogenic Engineering 37, 417(1992).

2. A.F. Zeller et al., MSU Annual Report (1990), p. 202.
3. J.A. Nolen et al., "A Proposal for Construction of the S800 Spectrograph", Technical Report MSUCL-694, National Superconducting Cyclotron Lab, July, 1989.
4. A.F. Zeller and J.A. Nolen, MSU Annual Report (1981-82), p. 90.

# CALCULATION OF 3D MAGNETIC FIELDS WITH ANSYS

D. Johnson, T. Kuo and F. Marti

Approximately one year ago we started using the commercial finite element code ANSYS [1] at our Laboratory. Given the very extensive capabilities of ANSYS (structural analysis, thermal analysis, etc) it seemed worthwhile to investigate the magnetic field calculation possibilities. A new kind of 3D Magnetic solid element, STIF96, had just been introduced as a beta test element. We decided to evaluate the accuracy of the code for magnets similar to our typical problems, cyclotron magnets, before accepting the results for new magnets where we did not have measurements. With that purpose, an old beam line dipole magnet was modified and equipped with sectored pole tips, and existing magnetic field mapping equipment was modified to be used with this magnet model. ANSYS utilizes [2] the difference scalar potential (DSP) formulation proposed by Mayergoyz, Chari and D'Angelo [3]. It avoids the numerical cancellation error of the reduced potential solutions and is continuous and unique across the interfaces.

In this formulation the first step is to calculate the magnetic field $\vec{H}_o$ under the assumption that the magnetic permeability of the iron volume is infinite, neglecting saturation. A difference field $\vec{h}$ is calculated as a perturbation to $\vec{H}_o$ due to saturation effects to give the the real field $\vec{H}$

$$\vec{h} = \vec{H} - \vec{H}_o \tag{1}$$

The DSP formulation requires the ferromagnetic region to be single-connected.

### Magnetic Field Measurements

The hardware utilized in the measurement has been described in previous reports [4]. Basically the system consists of a search coil that is moved radially through the center of the model towards the outside. The voltage generated by the changing flux is converted to pulses by a voltage to frequency converter. The number of pulses is then proportional to the magnetic field change between the center of the cyclotron (where it is determined by an NMR) and the observation point. The arm where the coil moves is then rotated to a new angular setting and the measurement repeated.

### Low Field Cyclotron Magnet

The low field magnet is an H-frame magnet with room temperature coils. It has mirror symmetry with respect to the $z = 0$ plane and also with respect to the $x = 0$ and $y = 0$ planes. The axis of the coils

is the z-axis. Due to these symmetries only one eighth of the magnet must be calculated, see Fig 1. The problem consists of 17301 active nodes with an RMS wave front of 489. The solution time in a VAX 3100/76

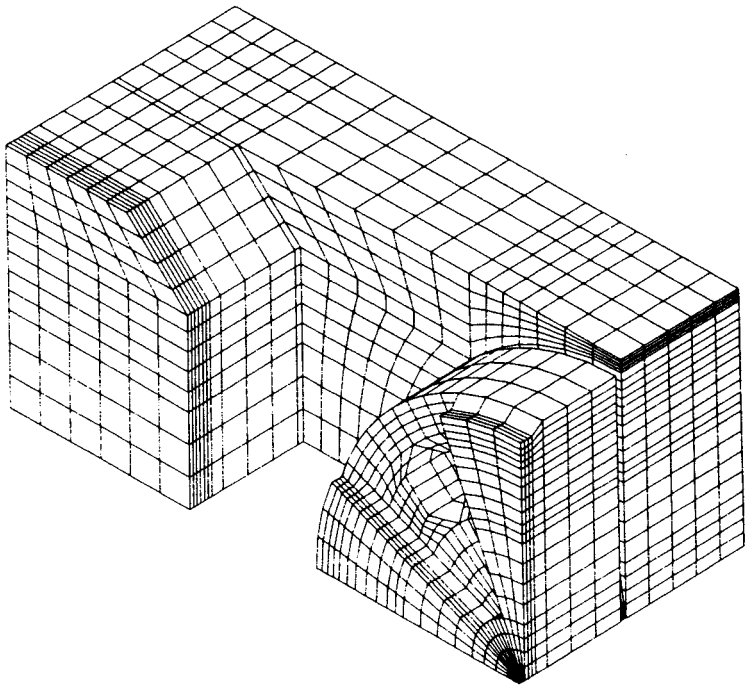

Figure 1: Mesh utilized for the calculation of the low field magnet. Only one eighth of the magnet is represented.

with 32 MBytes of memory was slightly less than 15 CPU hours. We display in Fig 2 the comparison of the main field parameters for the calculation and the measurement. The average field is shown at the top of the figure, where the calculation is shown to be about 0.03 T higher than the measurement. There is remarkably good agreement in the fourth harmonic. The observed discrepancies can possibly be attributed to uncertainties in the B -H curve of the steel. We tried to model this magnet with POISSON using an azimuthally symmetric magnet and using the stacking factors method but the results were drastically wrong.

### High Field Superconducting Cyclotron Magnet

To check the performance of the code in the high field region (5-6 T) we modelled the K1200 cyclotron. This accelerator is a three sector, variable energy, heavy ion machine, with very tight spiral shaped pole tips and superconducting coils. The maximum average field at extraction (r=1.0 m) is approximately 5 T and the third harmonic is 0.8 T. We already had the magnetic field measurements on a comprehensive grid used for the setting of the machine parameters.

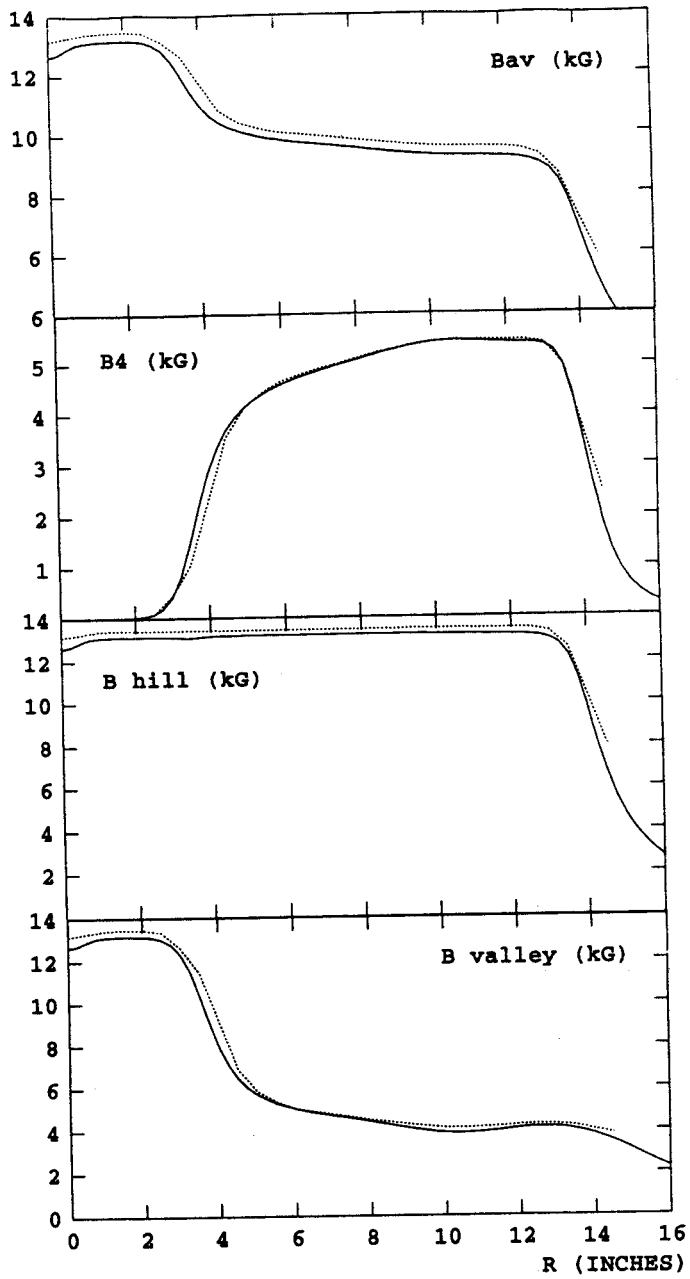


Figure 2: Comparison of the main field parameters in the median plane for the the calculation (dashed line) and the measurements (solid line). The average field, the fourth harmonic amplitude, the hill field and the valley field are shown as indicated.

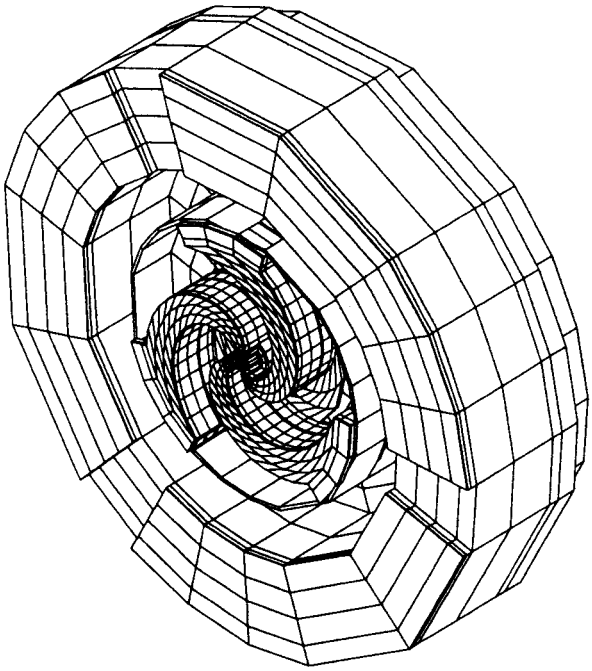

Figure 3: Mesh utilized for the calculation of the high field magnet. One half of the magnet is represented.

Due to the intricate geometry of the pole tips and the multiple holes in the yoke this is a complicated magnet to model, see Fig 3. The pronounced spiral of the pole tip near the edge gave us some difficulties. For this reason the mesh that we created is not a good representation of the real magnet in the region between r=0.8 and r=1.0 m. But we feel that it is good enough otherwise to check the accuracy of the model. This kind of compromise is common to all modelling problems, but a feature that we used that helps significantly is the possibility of using distinct meshes in adjacent regions with nodes that are not common. A provision exists for introducing constraint equations on the potential that can be found in an almost automatic way. The model consists of 10576 nodes, requiring a total of 23 CPU hours.

The results are compared in Fig. 4. As the yoke penetrations do not include all the holes in the yoke we expect the calculation to be higher than the measurements for the average field. The third harmonic is in very good agreement, but not so the sixth. This is understandable because the mesh is too coarse to obtain that kind of detail. We only have six points per sector in azimuth.

## Conclusions

The results of the low field calculation with ANSYS were in very good agreement with the measurements. The average field was 0.03 T higher than the measurements and a much smaller discrepancy was obtained in the harmonics. On the other hand the complexity of the problem in the

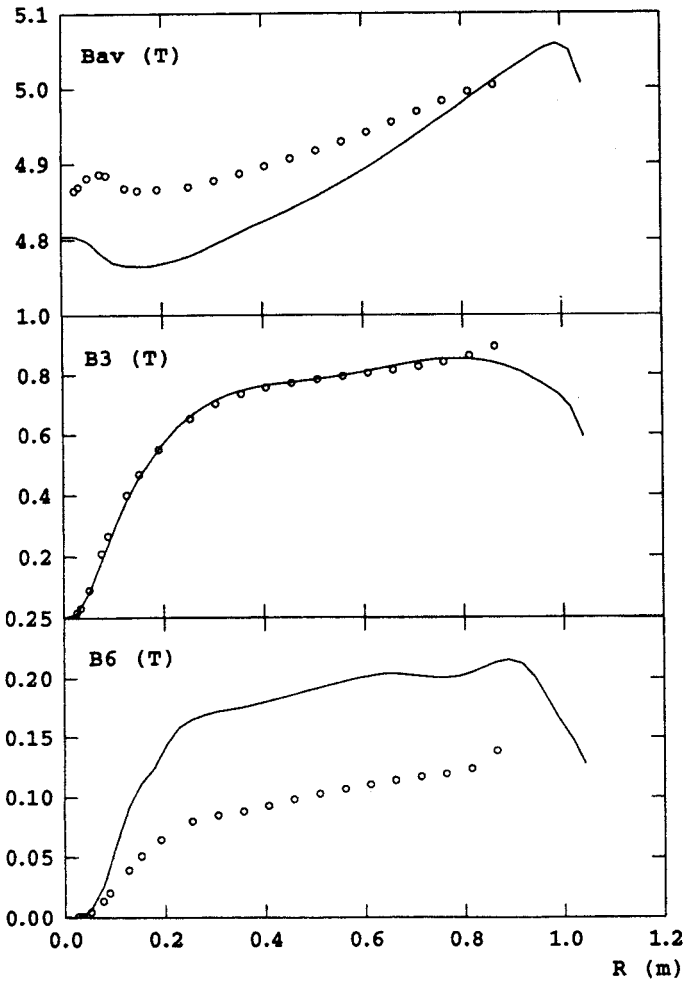


Figure 4: Comparison of the main field parameters in the median plane of the the calculation (circles) and the measurements (solid line) for the high field case. The average field and the third and sixth harmonic are shown.

high field case made it difficult to represent it with a reduced number of nodes. If one is willing to use more computer time the mesh could be refined and a better approximation obtained. This is a case where a POISSON calculation with stacking factors for the average field with a uniform magnetization approximation for the the harmonics could give a better result than a coarse 3D grid.

## References


1. Swanson Analysis Systems, Inc. Houston, PA 15342, USA.
2. D.F. Ostergaard and T.P. Pawlak, "Presentation of Team Workshop Problem No. 13", Unpublished, 1991.
3. I.D. Mayergoyz, M.V.K. Chari and J. D'Angelo, "A New Scalar Potential Formulation for Three-Dimensional Magnetostatic Problems", IEEE Transactions on Magnetics, Vol. MAG-23, No. 6, pp. 3889-3894, November, 1987.
4. L.H. Harwood and J.A. Nolen, in Proc. 10th Int. Conf. on Cyclotrons, (IEEE) 1984, p. 101.

# EVALUATION OF THIRD-HARMONIC VOLTAGE FLATTOPPING FOR A SUPERCONDUCTING CYCLOTRON

M.M. Gordon and Dong-o Jeon

Among cyclotron designers who aim at single turn extraction, the use of third harmonic voltage flattopping has long been recognized as a valuable tool for achieving higher beam currents while fulfilling the requirement of energy homogeneity within the extracted beam.[1] A very successful application of this technique has been achieved in the 600 MeV cyclotron at PSI(SIN) near Zurich.[2] More recently, experimental results have been reported on the use of a fourth harmonic voltage at the TRIUMF cyclotron.[3]

The K500 and K1200 superconducting cyclotrons at our laboratory have three magnet sectors with three dees in the intervening valleys. The interiors of two of these dees are occupied by cryopanels, while the remaining dee is vacant so that this space could be used to house a smaller dee that would provide a third harmonic voltage. The calculations reported here were designed to determine whether this project might be worth pursuing.

We used the simple differential equations for the longitudinal motion to find the energy $E$ and the phase $\phi$ as a function of turn number from given starting conditions. We then determined the range of initial phases $\phi_i$ for which the energy values on the final turn exceed the maximum energy of the previous turn. Within this phase range, the functional dependence of the final energy on the initial phase was optimized by adjusting the three available parameters: the amplitude and the relative phase of the third harmonic voltage , and the fundamental RF frequency. The availability of three parameters (rather than one) enables one to overcome the difficulties arising from the nonisochronous character of the magnetic field.

The electrode structures at the center of our cyclotrons are designed using the CYCLONE program which integrates orbits starting from the source (or inflector) using realistic electric fields. This process is based on the concept of a"central ray". That is, the central ray orbit is the one having the particular starting time which leads to the best overall energy-gain and which ends up with optimum centering. We assume that the current density as a function of starting time is symmetric about this value, and that the peak current density is associated with the central ray. When we compared the actual phase versus energy curve obtained from the CYCLONE program with curves obtained from the longitudinal motion

equations for different starting phases, we found that the best match occured for an assumed central ray starting phase $\phi_{ci} = -10°$. The calculations reported here therefore assumed this value. We also carried out calculations using $\phi_{ci} = 0°$, but the results were not significantly different.

The deviation of the magnetic field from isochronism, as determined from the equilibrium orbit code, is specified by the frequency error:

$$\Delta(E) = \omega_0/\omega - 1 = \nu_0\tau(E) - 1, \tag{1}$$

where $\nu_0 = \omega_0/2\pi$ is a given reference frequency, and $\tau(E) = 2\pi/\omega$ is the orbit period for a given energy. Figure 1 shows a plot of this function as derived from the K1200 field data for two cases:

$$E_f/A = 40 \text{ MeV} \text{ with } q/A = 0.25, \text{ and}$$

$$E_f/A = 200 \text{ MeV} \text{ with } q/A = 0.5,$$

where $E_f$ is the final energy, $qe$ is the ion's charge, and $A$ is its mass number. These curves show especially large values of $\Delta(E)$ near $E = E_f$ which result from the ions being accelerated out into the non-isochronous edge region of the field during the pre-extraction process.

During cyclotron operation, the RF frequency is adjusted as part of the optimization of the extracted beam current. We therefore set

$$\nu_{rf} = (1 + \epsilon)\nu_0, \tag{2}$$

where $\epsilon$ is an adjustable parameter. Note that $\epsilon$ values are generally very small and are given below in parts per million(ppm). Although we assume that the magnetic field is fixed, one could choose instead to make such adjustments by shifting the central field level.

Because of the electrode structures in the center of the cyclotron, the turn pattern is approximately fixed. If $qV_1$ is the peak energy-gain per turn produced by the first harmonic, we therefore set

$$qV_1 = E_f/n_0, \tag{3}$$

where $n_0$ is the nominal turn number. For the present calculations, we chose both $n_0 = 500$ and $n_0 = 800$, which are approximately the values appropriate for the K500 and K1200 cyclotrons.

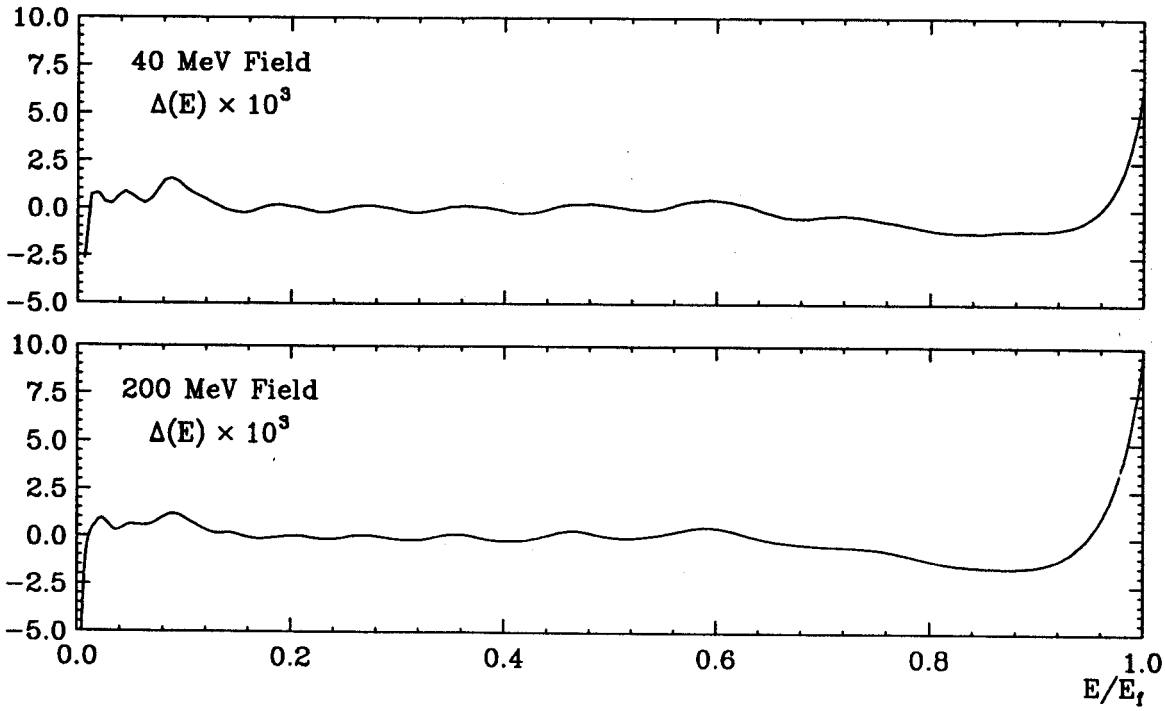


Fig. 1. Plots of the frequency error $\Delta = \omega_0/\omega - 1$ as a function of energy for two fields used to produce ions having the following final energies and charges: $E_f/A$=40 MeV with $q/A$=0.25(top), and $E_f/A$=200 MeV with $q/A$=0.5(bottom). The 200 MeV field is the least isochronous of all our fields.

The added third harmonic voltage is characterized by two parameters, the amplitude $V_3$ and the relative phase $\psi$. Instead of $V_3$, we use the dimensionless parameter $\lambda = V_3/V_1$ in our calculations. Thus the three available parameters are $\lambda$, $\psi$, and $\epsilon$.

The differential equations for $\phi$ and $E$ were integrated as a function of turn number $n$ starting from $n = 0$ with $E = 0$ and initial phase values $\phi_i$. For any parameter set $(\lambda, \psi, \epsilon)$, the integration proceeds until the central ray energy exactly matches the given final energy(e.g., 40 MeV), and this determines the final turn number $n_f$. The energy values for $n = n_f$ and different $\phi_i$ values are then examined to see if they meet certain criteria, and if not, a linear projection technique is used to obtain an improved parameter set. The entire process is iterated until which were distributed symmetrically about the central ray value the desired results are obtained.

As $\lambda$ increases above zero, the curve showing the final turn energy as a function of $\phi_i$ becomes broader and flatter, and when $\lambda$ exceeds a critical value $\lambda_c$, this curve exhibits two peaks rather than one. In this case, the parameters $\psi$ and $\epsilon$ are chosen so that the two peaks have the same height with the central ray in the valley midway between them. These conditions are consistent with our previously noted assumption concerning the symmetry of the current density as a function of starting time.

**Results**

Single turn extraction requires turn separation only at the final energy where the ions must clear the septum and enter the extraction channel. This radial separation of the turns at the final energy can be obtained provided the ion bunches are clearly separated in energy. That is, even if these bunches overlap spatially because of the radial oscillations, they can in principle be separated by a suitable dispersive process. In our cyclotrons as in many others, turn separation is generated by passage through the $\nu_r = 1$ resonance, and the amount of this separation is restricted by vertical stability requirements. This process has therefore limited dispersion.

In presenting our results here, we shall assume an energy spread within the bunch on the final turn, $\delta E$, which is just one-half of the peak energy gain on this turn. In this case, the energy gap between successive bunches is equal to $\delta E$.

Consider first the results obtained when the third harmonic is absent, i.e., $\lambda = 0$. For an isochronous field and a central phase $\phi_c \equiv 0$, one finds that the acceptable initial phase width is given by

$$\delta\phi_i = 2/\sqrt{n_0} \text{ (in radians)}, \tag{4}$$

where $n_0$ is defined in Eq. 3 above. For the two cases considered here, $n_0 = 500$ and $n_0 = 800$, this yields 5.1° and 4.1°, respectively.

The corresponding $\lambda = 0$ results were computed for the 40 MeV and the 200 MeV fields whose deviations from isochronism are shown in Fig. 1. For $n_0 = 500$, we found $\delta\phi_i = 4.8°$ and 4.7° for the 40 MeV and 200 MeV cases, while for $n_0 = 800$, we obtained $\delta\phi_i = 3.2°$ and 2.8° for the same two cases. Considering how small these values are, and considering also that the beam current is roughly proportional to $\delta\phi_i$, one can easily recognize the potential value of flattopping.

The greatest amplification of $\delta\phi_i$ is obtained for values of $\lambda > \lambda_c$ where the curve showing the final energy as a function of $\phi_i$ has two peaks. Following the procedure described near the end of the last section, and imposing the condition discussed above on the energy spread $\delta E$ within the bunch, we found the results that are summarized in the two tables below, one for $n_0 = 500$ and the other for $n_0 = 800$. In each table, data are presented for the two fields (40 MeV and 200 MeV) described in Fig. 1, and as a reference, for an isochronous field ($\Delta \equiv 0$).

These tables list the following items: the actual final turn number $n_f$; the RF parameters $\lambda$, $\psi$,

and $\epsilon$; the energy spread within the bunch as well as the energy gap between bunches, $\delta E$; and finally, the acceptable initial phase width $\delta\phi_i$.

Table 1 Results for $n_0 = 500$

| Field | Isoc | 40 MeV | 200 MeV |
|---|---|---|---|
| $n_f$ | 570.1 | 579.1 | 582.3 |
| $\lambda$ | 0.123 | 0.140 | 0.146 |
| $\psi$(deg) | 0.0 | 2.0 | 2.9 |
| $\epsilon$(ppm) | 97.5 | 91.6 | 101.3 |
| $\delta E/qV_1$ | 0.438 | 0.430 | 0.430 |
| $\delta\phi_i$(deg) | 35.4 | 34.2 | 33.5 |

Table 2 Results for $n_0 = 800$

| Field | Isoc | 40 MeV | 200 MeV |
|---|---|---|---|
| $n_f$ | 910.5 | 962.0 | 980.4 |
| $\lambda$ | 0.122 | 0.180 | 0.201 |
| $\psi$(deg) | 31.4 | 24.9 | 22.8 |
| $\epsilon$(ppm) | 61.1 | 66.5 | 85.9 |
| $\delta E/qV_1$ | 0.439 | 0.421 | 0.397 |
| $\delta\phi_i$(deg) | 31.4 | 24.9 | 22.8 |

The values of $\lambda$ given in the tables show that the required percentage of the third harmonic voltage rises from 12 for the isochronous field up to 14 or 15 for the two other fields when $n_0 = 500$. For $n_0 = 800$, however, this percentage rises from 12 up to between 18 and 20 in the same cases. These differences are quite significant when one considers the RF power requirement, and are due mainly to differences in the phase deviations. That is, the central phase $\phi_c$ ranges from $-10°$ to $+10°$ for the isochronous field, and from about $-30°$ to $+20°$ for the two nonisochronous fields when $n_0 = 500$. For $n_0 = 800$, on the other hand, the values of $\phi_c$ range from about $-50°$ to $+30°$ for the latter two fields.

The most impressive numbers in these tables are the values of $\delta\phi_i$. For $n_0 = 500$, the values for the two nonisochronous fields are less than $2°$ below the $\delta\phi_i$ for the isochronous field, and for all three fields, the values are about seven times larger than those given above for $\lambda = 0$. On the other hand, for $n_0 = 800$, there are significant differences between the $\delta\phi_i$ values for the isochronous and nonisochronous fields. One finds nevertheless that all these values are roughly eight times larger than those cited above for $\lambda = 0$ in the corresponding cases.

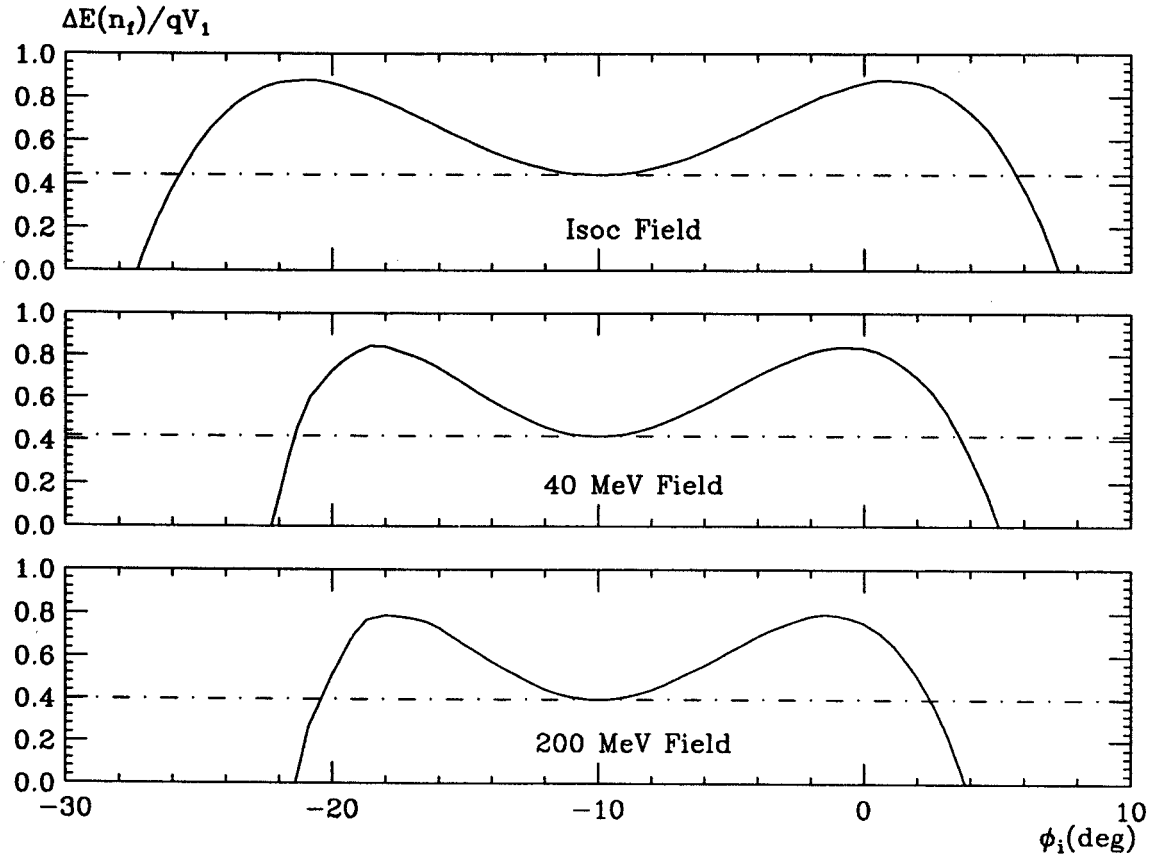


Fig. 2. Plots of the final energy as a function of the initial phase $\phi_i$ obtained under optimized conditions using the RF parameters given in Table 2 for three different fields: isochronous(top), 40 MeV(center), and 200 MeV(bottom). Here $\Delta E$ is the difference between the energy on the final turn and the maximum energy on the previous turn, and $qV_1 = E_f/n_0$ with $n_0 = 800$.

To illuminate the results further, plots of the final energy versus the initial phase are shown in Fig. 2 for all three fields when $n_0 = 800$. These curves show the two peaks of equal height with the central ray point ($\phi_{ci} = -10°$) in the valley midway between them. A horizontal broken line divides the full height into two equal halves each of height $\delta E$, as defined above. That is, the top half represents orbits within the final bunch while the bottom half shows the gap between successive bunches. The width of the curve where the straight line crosses it then defines $\delta\phi_i$, the acceptable initial phase width given in Table 2. Including the central ray itself, we therefore find three orbits which end up at $n = n_f$ with exactly the same energy.

Plots of the phase $\phi$ as a function of energy from $E = 0$ to $E = E_f$ are shown in Fig. 3 for the same three cases used in Fig. 2. The three solid curves correspond to the three orbits just mentioned which end up with the same final energy. The two intervening broken curves correspond to the orbits that end up

with the peak energy. These sets of curves show in detail the evolution of the phase deviations mentioned above. Curves similar to those shown in Fig. 2 and Fig. 3 were obtained for $n_0 = 500$, but these are less dramatic and are omitted here to save space.

While the K1200 cyclotron is fully occupied at present with carrying out nuclear physics experiments, the K500 cyclotron is available and could be used to test the effect of a third harmonic voltage on beam properties. As noted above, this cyclotron is characterized by a $n_0 = 500$ turn geometry and would, according to Table 1, require a third harmonic voltage which is about 14% of the first harmonic. Since only one of the three dees is available for the third harmonic voltage, this percentage rises to 42%. The design of a possible RF system is now under way.

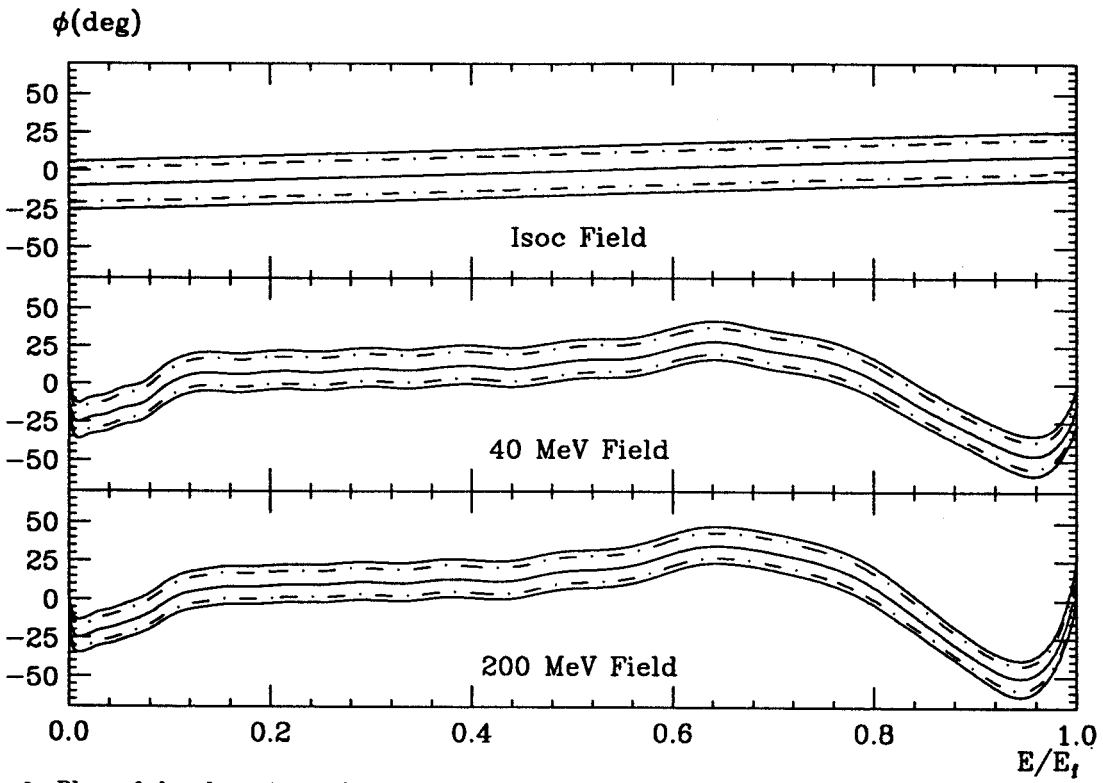


Fig. 3. Plots of the phase $\phi$ as a function of energy obtained for the same fields and RF parameters as those used for Fig. 2. The three solid curves all lead to the same final energy as defined by the horizontal broken line in Fig. 2, and the two broken curves lead to the two energy peaks in Fig. 2.

## References


1. M.M. Gordon, Nucl. Instr. & Meth. 58, 245(1968).
2. S. Adam, et al, IEEE Trans. NS-28, 2721(1981); W. Joho, Proc. Ninth Int'l. Cyclotron Conf. at Caen (Les Editions de Physique, Paris, 1981)337.
3. R.E. Laxdal et al, Conf. Record of the 1991 Particle Accelerator Conf. (IEEE 91 CH3038-7)810.

# NEW FEATURES IN COSY INFINITY

M. Berz, M. Zhao, W. Wan, and G. Hoffstätter

The beam physics design and simulation code COSY INFINITY [1] is a very versatile program which allows the study of nonlinear effects in accelerators and spectrographs in a very detailed way. It is based on differential algebraic techniques [2,3] and has a particularly user friendly interface based on an object oriented structured programming language. It consists of a compiler and executer for this language, written in plain FORTRAN 77 in order to run on a large number of systems, as well as a large collection of design and analysis tools for accelerators, particle spectrographs, beam lines, electron microscopes, and other beam physics devices.

Currently COSY INFINITY is used by about 70 registered users in 40 scientific laboratories all over the world. In 1991, two new releases, versions 4 and 5, were distributed to all the registered users by electronic mail. Besides minor maintenance, several important new features have been added.

COSY now allows the computation of high-order maps of Wigglers and Undulators. These devices are used in electron storage ring light sources to produce synchrotron radiation in a defined way by forcing the electron to oscillate in an alternating magnetic field. While their main function is the production of electromagnetic radiation, their influence on the motion of the particles is particularly important since they often introduce additional nonlinear effects. For their simulation, map methods are particularly fruitful since they allow a fast treatment of wigglers, while numerical integration techniques are usually particularly slow because the oscillatory form of the dynamics, is more complicated than in standard elements.

There are also new routines which allow the simulation of cavities as they appear in accelerators. Cavities are the main source for the coupling of the two conventional phase space planes with the longitudinal motion. Furthermore, there are now routines that allow the use of superimposed skew multipoles. Finally, it is now also possible to compute the transfer maps of Wien filters. These are devices with superimposed electric and magnetic deflection fields, which are often used as velocity filters.

The normal form methods [4], which provide a powerful tool to study the nonlinear behaviour of repetitive systems, have been upgraded to allow the computation of resonance strengths. These characteristics for the importance of nonlinear resonances flow naturally out of the normal form concept,

and they allow a rather straightforward correction of nonlinear lattices. They were used recently for the adjustment of correction sextupole strengths both for the SSC low energy booster and the TRIUMF KAON rings.

Finally, there is now a translator from one of the most important standards to describe accelerator lattices, the MAD language, to the input of COSY INFINITY. This translator, which was developed mostly by Roger Servranckx, a COSY user at TRIUMF, considerably facilitates the use of the program for the large accelerators for which MAD inputs exist and often allows their study with COSY within a few minutes.

## References


1. M. Berz, COSY INFINITY Version 5 reference manual, Technical Report MSUCL-811, National Superconducting Cyclotron Laboratory, Michigan State University, East Lansing, MI 48824, 1991.
2. M. Berz, Differential algebraic description of beam dynamics to very high orders, *Particle Accelerators*, 24:109, 1989.
3. M. Berz, Arbitrary order description of arbitrary particle optical systems, *Nuclear Instruments and Methods*, A298:426, 1990.
4. M. Berz, *High-Order Computation and Normal Form Analysis of Repetitive Systems, in: M. Month (Ed), Physics of Particle Accelerators.* American Institute of Physics, 1991.

# DESIGN OF THIRD ORDER ACHROMATS

E. Goldmann and M. Berz

The question if there are systems without any aberrations up to a certain order, so-called achromats, is an old and fundamental problem of optics. While it is not very difficult to design first order achromats, the correction of all second order aberrations already represents a major effort [1]. It turns out that to eliminate aberrations, it is very advantageous to employ certain symmetries of the systems, and so most second order achromats consist of four identical cells which are either placed in series or appear in various mirror symmetries.

In the past years, various third order achromatic systems consisting of only repetitive arrangements of identical cells have been found using normal form theory. The first such system, which was more or less a proof of principle, consisted of thirty identical cells and a total of 150 bending magnets [2]. Recent work of Neri [3] produced a much more feasible system consisting of five identical cells placed in series.

Since the number of cells required directly influences the complexity of the device, it is desirable to reduce the number of cells as much as possible. Here we discuss a new series of third order achromatic systems which contain only four cells, each of which requires only one bending magnet. They are based on an entirely new approach to find a classifications of achromatic systems analytically.

Instead of using identical cells as in the normal form approach, we utilize cells which are obtained from the original ones through mirror imaging about the $x$-$y$ plane, which corresponds to a reversion, cells which are obtained through mirror imaging about the $x$-$z$ plane, which corresponds to a switching of the bending direction, and those which are obtained through both of these mirror imaging processes from the original cell. We denote the original forward cell with F, the reversed cell with R, switched cell with S, and the combined switch-reversed cell with C. (Fig. 1). To obtain achromatic systems, we use combinations of these cells which are derived from a forward cell F with suitable aberrations removed.

In order to study the nonlinear behaviour of the combined systems, we have to take into account the inter correlations between the aberrations of the map which are connected to the condition of symplecticity [4], a direct consequence of the Hamiltonian structure of the motion. To this end, the map $\mathcal{M}$ of the forward cell is represented in the form

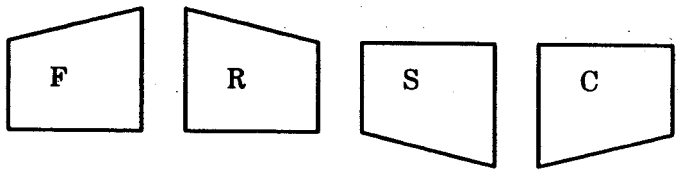


Figure 1: Forward (F), Reversed (R), Switched (S) and Combined Switched-Reverse (C) Cells

$$\mathcal{M} = M \circ \exp(: H :) \tag{1}$$

where $M$ is the linear part of the and $H$ is a polynomial of exact order 3 and 4 describing the nonlinear part of the map [5]. The goal is now to demand that certain terms in $H$ vanish in such a way that the total system is free of aberrations.

In an extensive analytical computer search carried out with COSY INFINITY, we first studied all possible first order rotation maps $M$ which can produce a first order achromat. For each of these, all possible combinations of arrangements consisting of the four elementary cells F, R, S, and C were considered. For each of these combinations, it was determined in an analytical way which terms in $H$ of the forward cell have to be removed to obtain a third order achromat. We first test every term in the Hamiltonian by setting all the other terms to zero to see if it produces aberrations. If it does, it means the coefficient certainly has to be fit to zero. In the end, all monomials which passed the first test are given 16 digit random numbers coefficients, and it is checked if the resulting linear combination still produces an aberration free system. If that is the case, the system represents a true achromat beyond reasonable doubt, or to be precise with a probability of about $1 - 10^{-16}$, which is determined by the probability of producing an accidental zero in a sequence of operations with random numbers.

After extensive computer searches involving the analytical study of millions of systems and requiring hundreds of hours of CPU time, we found the following family of third order achromats, all of

which require the removal of the same terms in the polynomial $H$. Table 1 lists the terms which have to be removed. If in addition to being free of aberrations, it is also desired to remove all dependencies of final angles on initial quantities, other terms have to be killed, which are listed in Table 2. Depending on the choice of the linear chromatic property of the forward cell, various arrangements of cells yield achromats. These are listed in Tables 3 and 4, each entry of which describes a pair of rotation angles for the $x$ and $y$ maps which produces an achromat.

| | | | | |
|---|---|---|---|---|
| $xa^2$ | $a^3$ | | | |
| $xb^2$ | $ayb$ | $ab^2$ | | |
| $a^2\delta$ | $b^2\delta$ | | | |

| | | | | |
|---|---|---|---|---|
| $x^2a^2$ | $a^4$ | | | |
| $xayb$ | $x^2b^2$ | $a^2y^2$ | $a^2b^2$ | |
| $y^2b^2$ | $b^4$ | | | |
| $a^2\delta^2$ | | | | |
| $b^2\delta^2$ | | | | |

Table 1: Second and third order kills necessary to obtain a third order achromat

| | | | | |
|---|---|---|---|---|
| $x^3$ | $xa^2$ | | | |
| $xy^2$ | $xb^2$ | $ayb$ | | |
| $x^2\delta$ | $x\delta^2$ | $a^2\delta$ | $y^2\delta$ | $b^2\delta$ |

| | | | | |
|---|---|---|---|---|
| $x^4$ | $x^2a^2$ | $a^4$ | | |
| $x^2y^2$ | $xayb$ | $x^2b^2$ | $a^2y^2$ | $a^2b^2$ |
| $y^4$ | $y^2b^2$ | $b^4$ | | |
| $x^2\delta^2$ | $a^2\delta^2$ | | | |
| $y^2\delta^2$ | $b^2\delta^2$ | | | |

Table 2: Second and third order kills necessary to obtain a third order achromat which is also free of angle aberrations

Obviously the employed mirror symmetry has merits and drastically reduces the number of fitting conditions. We need only to cancel 7 out of 19 third order terms and 10 out of 37 fourth order terms in the Hamiltonian to get a third order achromat. Even if we want a so called full third order achromat which has no aberration in both $x$,$y$ and $a$,$b$ columns, the conditions show that it is still feasible(10 third terms and 15 fourth order ones, Tab. 3 and Tab. 4).

Currently work is under way to try to design a realistic third order achromat following the results

| $\theta_x$ | $\theta_y = 0$ | $\theta_y = 90$ | $\theta_y = 180$ | $\theta_y = 270$ |
|---|---|---|---|---|
| 0 | F C S R | F C S R | F C S R | F C S R |
| 90 | F C F C | F C F C | F C F C | F C F C |
| 180 | F C S R | F C S R | F C S R | F C S R |
| 270 | F C F C | F C F C | F C F C | F C F C |

Table 3: Systems with $(x|\delta) = 0$

| $\theta_x$ | $\theta_y = 0$ | $\theta_y = 90$ | $\theta_y = 180$ | $\theta_y = 270$ |
|---|---|---|---|---|
| 0 | F R S C | F R S C | F R S C | F R S C |
| 90 | F R F R | F R F R | F R F R | F R F R |
| 180 | F R S C | F R S C | F R S C | F R S C |
| 270 | F R F R | F R F R | F R F R | F R F R |

Table 4: Systems with $(a|\delta) = 0$

described above. The first order map under study is based on $\theta_x = 180deg$, $\theta_y = 90deg$ and $(a|\delta) = 0$.

## References


1. R. V. Servranckx and K. L. Brown, Circular machine design techniques and tools, *Nuclear Instruments and Methods*, A258:525, 1987.
2. A. J. Dragt. Elementary and advanced Lie algebraic methods with applications to accelerator design, electron microscopes, and light optics; *Nuclear Instruments and Methods*, A258:339, 1987.
3. M. Berz F. Neri and J. McIntyre (Eds.), Proceedings of the 1990 workshop on high order effects in accelerators and beam optics, Technical Report MSUCL-767, National Superconducting Cyclotron Laboratory, Michigan State University, East Lansing, MI 48824, 1991.
4. H. Wollnik and M. Berz, Relations between the elements of transfer matrices due to the condition of symplecticity, *Nuclear Instruments and Methods*, 238:127, 1985.
5. M. Berz, COSY INFINITY Version 5 reference manual, Technical Report MSUCL-811, National Superconducting Cyclotron Laboratory, Michigan State University, East Lansing, MI 48824, 1991.

# FRINGE FIELD APPROXIMATIONS

G. Hoffstätter and M. Berz

The fringe fields of particle optical elements have a strong effect on optical properties. So far their transfer maps can only be calculated accurately using numerical integrators, which is very time consuming. We developed a new symplectic approximation method and implemented it in COSY INFINITY [1].

Often the effect of fringe fields is approximated by fringe field integrals to save computation time. This was done in second order for TRANSPORT [2] and in third order for GIOS [3]. There is an attempt being made to expand to fifth order [4] for some particle optical elements. The approximation by fringe field integrals, however, has some serious disadvantages:

- It is non-symplectic and therefore not especially suited for circular machines, where symplectic tracking can be advantageous.
- It represents the fringe effect well only if the region of the fringe field is not much bigger than the dimension of the beam diameter.
- It is restricted to low orders.

In order to speed up the fringe field calculation in the arbitrary order code COSY INFINITY we searched for a method that does not have those drawbacks, works fast, and to all orders.

In the following we will use TRANSPORT notation for the map [5], which means the variables of motion are the cartesian coordinates and slopes $x, x', y, y'$, the path length difference $l$, and the relative momentum deviation from a reference momentum $\delta_p$. Those six components build the vector $\vec{z}$. The transfer map describes the variables of motion $\vec{z}_f$ behind an optical element as a function of the variables $\vec{z}_i$ in front of it.

$$\vec{z}_f = \vec{M}^P(\vec{z}_i) \tag{1}$$

The index $P$ indicates that the map $\vec{M}$ depends on certain parameters, like the momentum $p$, mass $m$, and charge $z$ of the reference particle and the aperture $A$ of the optical element.

From now on we will be concerned with magnetostatic elements, although parts of the procedure are applicable to electrostatic elements, too. The equation for the Lorentz force yields that the bending

radius of the path of a particle with momentum $p$ at field $B$ is

$$R = \frac{p}{qB\sin\phi} \tag{2}$$

where $\phi$ denotes the angle between momentum and field direction. All maps are identical that describe particles with equivalent bending radii along their path. If the map for a specific beam is known as a function of the field $B$ at the pole tip, the transfer map for all other beams can be computed:

$$\vec{M}^{p^*,m^*,z^*,B^*} = \vec{M}^{p,m,z}(B)|_{B=B^*\frac{z^*p}{p^*z}} \tag{3}$$

The map on the right hand side is known as a function of the field $B$, whereas the left hand side describes a map that is calculated at a certain field $B^*$. This is just another way of saying that the map depends only on the ratio of field $B$ to magnetic rigidity $p/z$, as long as saturation is not important. At this point it is important to use TRANSPORT notation with $\delta_p$ as a variable, rather than the relative energy deviation $\delta_E$, because the relative momentum deviation is equivalent to a relative deviation from the bending radius at momentum $p$ as well as at any momentum $p^*$. Therefore the dependence of $\vec{z}_f$ on $\delta_p$ is the same at $p$ and at $p^*$. With $\delta_E$ as a variable this would not be the case. Furthermore it is helpful that the TRANSPORT notation uses path length as a variable, rather than time of flight, because the time of flight is different for different reference momenta, whereas the path length stays the same.

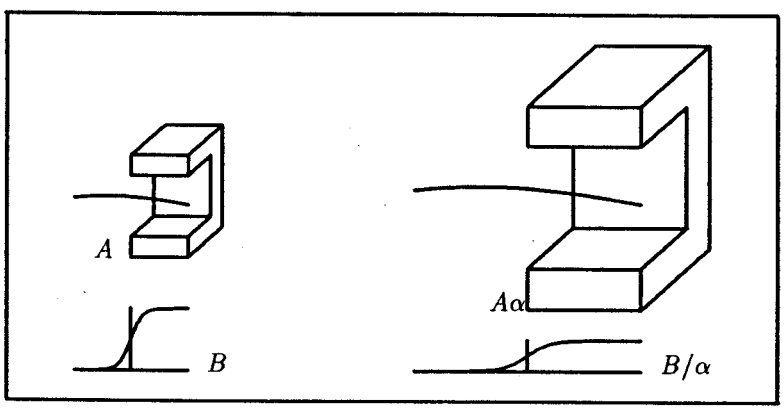


Figure 1: Particle coordinates in two elements scale with a factor $\alpha$, if the elements scale with a factor $\alpha$, and the fields scale with a factor $1/\alpha$ .

Now let us consider two similar magnetostatic elements that differ by a scaling factor $\alpha$, only. If the bending radii also differ by a factor of $\alpha$, the maps are similar. Equation (2) shows that this is the case

whenever the $\alpha$-times bigger element has a $1/\alpha$ times stronger field. After scaling the coordinates $x, y, l$, we obtain

$$\begin{pmatrix} M_x^{B/\alpha,A\alpha} \\ M_{x'}^{B/\alpha,A\alpha} \\ M_l^{B/\alpha,A\alpha} \\ M_{\delta_p}^{B/\alpha,A\alpha} \end{pmatrix}_{(x_i,x_i',l,\delta_p)} = \begin{pmatrix} \alpha M_x^{B,A} \\ M_{x'}^{B,A} \\ \alpha M_l^{B,A} \\ M_{\delta_p}^{B,A} \end{pmatrix}_{(x_i/\alpha,x_i',l/\alpha,\delta_p)} \tag{4}$$

The second dimension $(y, y')$ is not mentioned, for it has the same properties as $(x, x')$.

As a conclusion, we state that the knowledge of the transfer map as a function of the field strength at the pole tip, for particles with a specific magnetic rigidity, and for an element with a specific aperture, is sufficient to know all transfer maps of similar elements, for all energies, masses, and charges. In fact the map does not even have to be known as a function of the field, because the dependence on the field can be obtained by equation (3) from the dependence of the map on the momentum, which is already contained in the map, as momentum is one of the six variables.

In general it is useful and customary to work with the canonical coordinates $(x, \frac{p_x}{p_0}, y, \frac{p_y}{p_0}, \frac{E_0}{p_0}(t_0 - t), \delta_E)$ [6], therefore a transformation routine had to be implemented that transforms canonical notation into TRANSPORT notation and back.

$$M^{p,z} = T_{(E,m)} M^{E,m,z} T^{-1}_{(E,m)} \tag{5}$$

This transformation $T$ depends on the reference energy and mass.

COSY INFINITY can readily compute the map of a fringe field of certain aperture $\vec{M}^{E,m,z,A}$, with $\delta_E$ being the sixth variable. Now we would be finished. The map $\vec{M}^{E,m,z,A}$ of a certain fringe field for a certain beam had to be stored once as a function of $B$ in order to compute maps of similar fields and all kind of beams. COSY INFINITY, however, can only approximate a function by its Taylor series, therefore the scaled map will only be approximated. The accuracy depends on the chosen order of the Taylor expansion and on the relative difference of the bending radii in the scaled and the saved element. We can live with that for we only strive for an approximation. The approximated map will only be approximately symplectic. Symplecticity, however, is an intrinsic symmetry of canonical motion that arises from the special structure of Hamilton's equations. It should not be violated, especially when long term behaviour is of interest.

This drawback can be eliminated by storing the reference map $\vec{M}^{E,m,z,A}$ in a symplectic representation [7]. Either in form of a generating function

$$\vec{z}_{i,f} = SJ\partial_{\vec{z}_{i,f}} F(B) \tag{6}$$

where $S$ is a matrix with only 1 or $-1$ on the diagonal, or in form of a Lie factorization

$$\vec{z}_f = L(B)e^{:P(B):}\vec{z}_i \tag{7}$$

where $:P:$ denotes a Poisson bracket waiting to happen. In higher orders the first representation is slow because a map inversion is required. The second one has the disadvantage that the matrix L(B) can only be approximated and is not exactly symplectic. It is most efficient to represent the non-linear part by $e^{:P:}$ and the linear part by the generating function that is most accurate for the given matrix L.

Now all pieces are assembled to display figure (2) which describes the whole symplectic scaling procedure. To do the required manipulation of parameter dependent maps certain procedures like the Lie transformation, the generating functions, and the TRANSPORT notation had to be added to COSY INFINITY.

Figure (3) shows the dependence of the expansion coefficient $(x, xxa)$ as a function of the field $B$ at the pole tip of a quadrupole. Because functions like this can be closely approximated by polynomials, this procedure is quite accurate. The following speed and accuracy comparisons will be made to the standard COSY Runge Kutta of eighth order which for the sake of speed is usually set to an accuracy of $10^{n-9}$ for order $n$. This integrator is thought to be most efficient for the differential equations of particle dynamics [8]. Even at the border of the range in figure (3), the presented method is more accurate than the COSY standard integrator. Inside the region the accuracy increases drastically. The results in figure (3) were obtained by evaluating the symplectic reference representation to third, fourth, and fifth order. The accuracy can be further improved by increasing this order which of course increases the computation time that has to be invested for creating the reference map in advance. This investment can be very much rewarding, especially when beamlines or spectrometers are being fitted so that maps of similar fringe fields are needed over and over again with only slightly different parameters.

In typical cases the presented method is faster by a factor of 45 for first order and 80 for third order matrix elements, for higher orders the speed advantage increases rapidly.

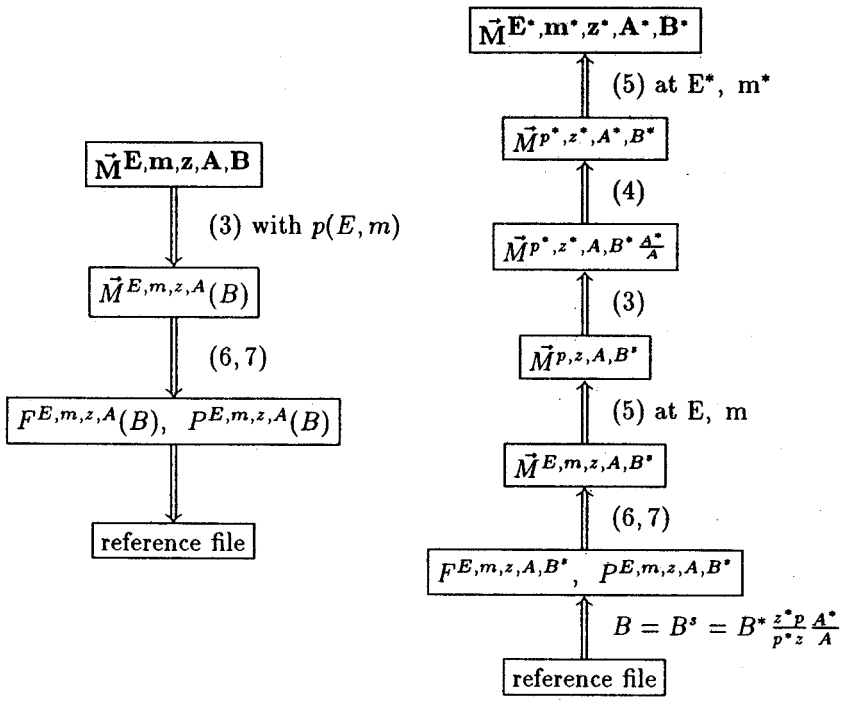


Figure 2: Shows how a map for arbitrary beam parameters $E^*, m^*, z^*$, fields $B^*$, and aperture $A^*$ can be computed from the map of a similar element using symplectic scaling.

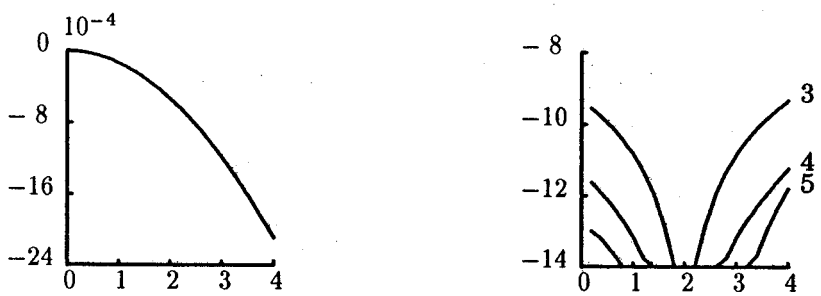


Figure 3: left: $(x, xxa)$ for a quadrupole as a function of the field at the pole tip. right: Logarithmic error of the approximation of $(x, xxa)$ with different expansion orders for the reference representation. The reference representation was computed at $B = 2T$.

## References


1. M. Berz, COSY INFINITY, In *Proceedings 1991 Particle Accelerator Conference*, San Francisco, CA, 1991.
2. R. H. Helm, First and second order beam optics of a curved inclined magnetic field boundary in the impulse approximation, Technical Report 24, SLAC, 1963.
3. H. Wollnik, J. Brezina, and M. Berz, Space charge effects in final focusing systems in *Proceedings INS International Symposium*, Tokyo, 1984.
4. B. Hartmann, To appear in 1992 Proceedings International Workshop to Nonlinear Problems in Accelerator Physics, 1992.
5. K. L. Brown, A first- and second-order matrix theory for the design of beam transport systems an charged particle spectrometers, Technical Report 75, SLAC, 1982.
6. M. Berz, Computational aspects of design and simulation: COSY INFINITY, *Nuclear Instruments and Methods*, A298:473, 1990.
7. M. Berz, Arbitrary order description of arbitrary particle optical systems, *Nuclear Instruments and Methods*, A298:426, 1990.
8. Ingolf Kübler, Master's thesis, Justus Liebig Universität Gießen, 6300 Gießen, West Germany, 1987.

# MEDICAL CYCLOTRON CONTROL SYSTEM UPGRADE

G.Zheng, R.Morin, and H.Blosser

The K100 medical cyclotron ran successfully in 1991 for various beam experiments and patient treatment. The control system has undergone upgrades to meet operational requirements and improve overall cyclotron performance. Changes involving the rf control were discussed in the paper published in last year's annual report. Further rf control modifications to the Dee Voltage Controller to be compatible with rf pulsing and a new phase detector that will allow higher dc gain are described here. Also discussed are some control software changes and a newly developed Console Interlock System which will allow direct control of the cyclotron from the treatment console and at the same time greatly improve the system operational safety.

## Dee Voltage Controller Modification

The main function of the Dee Voltage Controller (DVC) module is to generate a pulse to control the rf. As shown in the Dee Voltage Control Signal Flow Diagram (Fig.1), when the DVC pulse comes on, the rf signal from the source module will be applied to the rf pre-amplifier (802A Exciter), the rf power will be enabled and thus the dee voltage will build up. When the DVC pulse goes off, the source rf signal will be muted, turning off the rf power and thus the dee voltage will decay to zero.

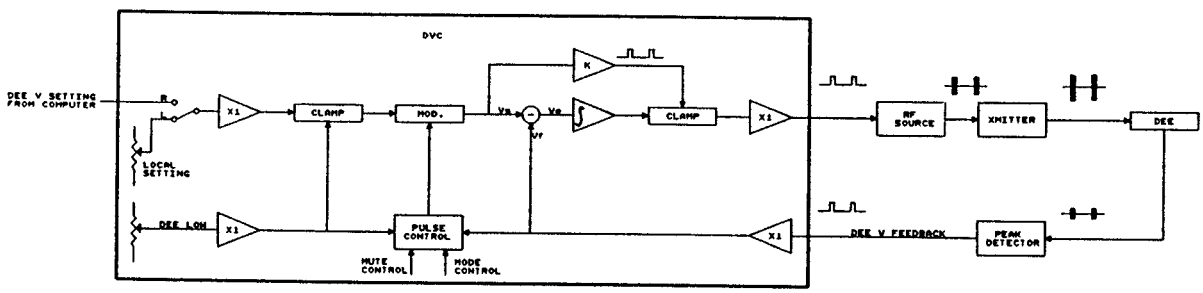


Fig. 1. DVC AND THE RF CONTROL

In the previous DVC design, the pulse controlling the rf had a fixed 10V amplitude, independent of the 0-10V adjustable reference that sets the dee voltage. With this arrangement the rf was turned on at its full power of 25KW and later dropped to whatever the dee voltage setting required. This caused the dee voltage to overshoot and was sometimes unstable, especially when running at a low beam energy.

To solve this problem, a new DVC design with a different control scheme was adopted. Instead of using the 0-10V dc as the dee voltage setting reference, the DVC first modulates the reference dc with the rf control pulse, then uses this modulated signal for both the dee voltage setting and the initial pulsing. Thus the amplitude of the rf turn on pulse is dee voltage setting dependent. To break through multipactoring, a gain control circuit allows a moderate amount of overshoot to be added to the initial pulse. A Dee Low Clamping circuit cuts the pulse off when the setting is too low. To make the pulse control easier, the new design uses independent frequency and duty cycle adjustment, directly accessable from the DVC front panel. To avoid coherrent noise interference introduced by the ac line voltage, the rf control pulse has been changed from 60Hz, 3.3mS to 100Hz, 2.0mS.

**RF Phase Control Upgrade**

The rf detector module currently being used consists of two peak detectors and one phase detector. The module was originally designed for continuous rf and later modified to work with the pulsed rf. This affected the phase detector because its average dc output was reduced by a factor of five due to the 20% pulse duty factor. If not compensated properly, the phase loop control precision would be reduced. Theoretically the compensation can be easily done by either reducing the BBS window width setting or increasing the phase detector dc gain. Practically, however, reducing the window width setting is not feasible because the setting is already small (0.27V), and further reduction will not help much and may cause the trimmer to oscillate. On the other hand, increasing the phase detector dc gain was limited by the exsisting circuit arrangement. The dc gain control amplifier is preceded by the phase detector and followed by the offset control and the Low Pass Filter (LPF). Thus the pulse modulated phase output will be amplified before being dc shifted and filtered. This limits the achievable gain increase due to amplifier saturation. Acceptable performance has been obtained but the dynamic range needs to be expanded beyond that possible with the current design.

A new phase detector with different signal flow path has been designed and built, which will allow the pulsed phase output to be properly shifted and converted to dc before being scaled up with higher gain. The new detector also has better input isolation because of two unit gain buffers, one for each rf phase signal, inserted in between the Zero Crossing Detector (ZCD) and the input attenuator. The new design also packages the peak detectors and the phase detector in separate units so each one can be independently replaced. The new design will be installed in the system and tested as soon as sufficient system time is available.

Another rf phase control system upgrade involved the solid state relays that control the rf trimmer drive. They failed every time a high intensity beam was run. The relays were packaged inside

the Trimmer Local Control (TLC) box, which is mounted very close to the cyclotron. Neutron damange is likely the reason that the relays failed. To solve this problem, the relays were removed from the TLC box and repackaged into a new module called the Drive Relay Module (DRM). The DRM is mounted on the control rack in the utility room a significant distance away from the cyclotron. Since the relocation, no failure has been reported.

### Console Interlock System

Currently the K100 medical cyclotron radiation safety protection is achieved through a relay contact signal called Area Cleared that is generated by the Room Survey System (RSS). The signal is routed to the Cyclotron Control System (CCS) and used to turn off the cyclotron when excessive neutron radiation is detected or the working area is not secured. Enhanced safety margin can be realized by employing redundant signals and implementing backup protection using the RSS and the CCS. Also it is desired to allow direct control of the cyclotron from the treatment console which requires communication between the treatment console and the cyclotron console. To meet these requirements, the Console Interlock System (CIS) was developped, which includes the newly designed Console Interlock Module (CIM) and the modified Safety Interlock module (SIM), as shown in the Fig.2.

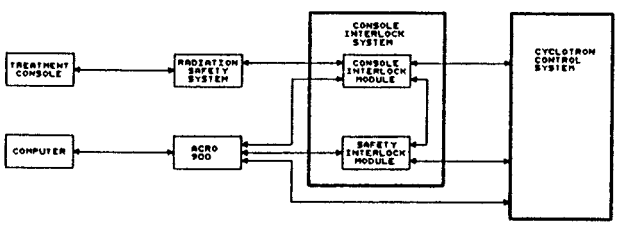


Fig. 2. CONSOLE INTERLOCK SYSTEM

The CIM has three major functions: First, it will interface four RSS interlock signals to the computer for radiation safety protection. Simultaneously the CIM built in logic circuit will generate relay contact signals to disable the transmitter and the source power supply control when an interlock occurs. Software interlocks will provide backup protection. Secondly, the CIM will set up communications between the treatment console and the computer console so operators can directly control the cyclotron from the treatment console, and read several important control status signals there as well. Finally, the CIM also provides a Key Lock circuit. The Key Lock circuit is actually an interlock circuit that requires operators to get permission to access the cyclotron control by first unlocking a safety key switch. There are three key switches in the system, one assigned to each control location, i.e. the treatment console, the computer console and the control panel. One and only

one key switch at a time can be turned on or cyclotron operation is inhibited. This will make operation safer and allow control to easily move from one place to another.

The SIM must be modified to work with the CIM in fulfilling the above control tasks. Its most important function of watch-dog timer will be preserved. The watch-dog timer was designed to monitor the computer control, and sends a signal to immediately turn off the cyclotron should the computer control fail. The Console Interlock System has been developed and will be evaluated before final installation.

## Control Software Modifications

The control software has undergone three significant changes over last year. The first change was a modification to permit limited control of the cyclotron from the treatment console and the operation of the CIS. To accomplish this, additional discretes were added to communicate with the treatment console and the conditions for control of the transmitter and ion source were revised. Serveral of the screens available on the computer were changed to be compatible with the revised procedures and interlock conditions.

The second change added an automatic initial rf trimmer set capability as a function of gantry position. When the automatic mode is active the trimmer will be automatically set to a position calculated from a polynomial fit to eight calibration points. The values at the calibration points are entered via the keyboard and are preserved over intervals when the control system is turned off.

The software was also revised to allow six more logging channels so operators could easily track more cyclotron parameters. The new parameters include two channels for cryoline and cryobox vacuum readings, three channels for the coil pressure, the fill valve pressure and the suction pressure and one channel for the coil lead drop reading.

## Conclusion

The efforts spent in upgrading the K100 medical cyclotron control has improved system overall operational performance measures such as the controllability and reliability. The machine is now running smoothly with no major break down during the last six months.

# WEAR STUDIES SUMMARY

H.J. Schock, D.A. Barkmann, Y. Chung, D.S. Grummon, R. Schalek,
R.M. Ronningen, Wm.C. McHarris, and H. Tsieh

In last year's annual report our group described preliminary results on determining radiation damage after ion implantation. Martinsitic stainless steel and silicon nitride were irradiated with 2.5 Mev/u $^{20}Ne^{2+}$ ions, with doses of $2\times10^{12}$, $2\times10^{13}$ and $2\times10^{14}$ ions. The purpose of the study was to simulate the implantation of radioactive ions, which would serve as tracers in tribological studies. For doses that would be useful in tribology studies using the radioactive ion implantation technique no damage was observed.

One facet of our study was examined more closely this year[1]. The measured damage site did not match ion depth calculations predicted by the code TRIM-91[2]. The predicted implanted ion concentration profile centroid is about 10.6 microns for the above ions, and the lattice damage profile centroid is about 10.4 microns. Our study showed the damage occurred at about 16 microns for the only dose in which damage was observed, $2\times10^{14}$ ions/cm$^2$. We speculated that, owing to the split samples, surface roughness played a role in this discrepency. This is depicted in Fig. 1. To test this hypothesis, the "B" surface of the irradiated sample was mechanically ground and polished. Another set of nanoindentation studies was done. The results are shown in Fig. 2. The profiles show damage depths in agreement with TRIM-91 predictions. And, in agreement with our earlier analysis, no evidence for damage was observed for the lower doses.

Investigations are underway to determine reactions which will produce $^7Be$ more prolifically than the projectile fragmentation reaction. A test of the p($^7$Li,n)$^7$Be reaction at 5 MeV/u was performed using a $^7Li^{2+}$ beam from the K500 cyclotron. Polyethylene targets were used. At 5 Mev/u the reaction cross section is nearly an order of magnitude larger than the projectile fragmentation cross sections for $^7Be$ production. In the Li-induced reaction, the $^7Be$'s are kinematically limited to angles smaller than 7 degrees in the laboratory. Their range is useful for wear studies, being about 70 microns in aluminum, and their energy spread is relatively small (12 MeV). In this test, the $^7Be$'s were implanted in a foil stack of aluminum placed immediately behind the target. The beam also stopped in the foil stack, but few $^7Be$'s were attributed to the interaction between $^7Li$ and $^{27}Al$. For actual implantations it will be desireable to separate the $^7Be$'s from the beam. The magnetic rigidities of the beam and the $^7Be$'s differ by approximately 50% and are small in magnitude. Therefore, a relatively inexpensive separation scheme should be possible.

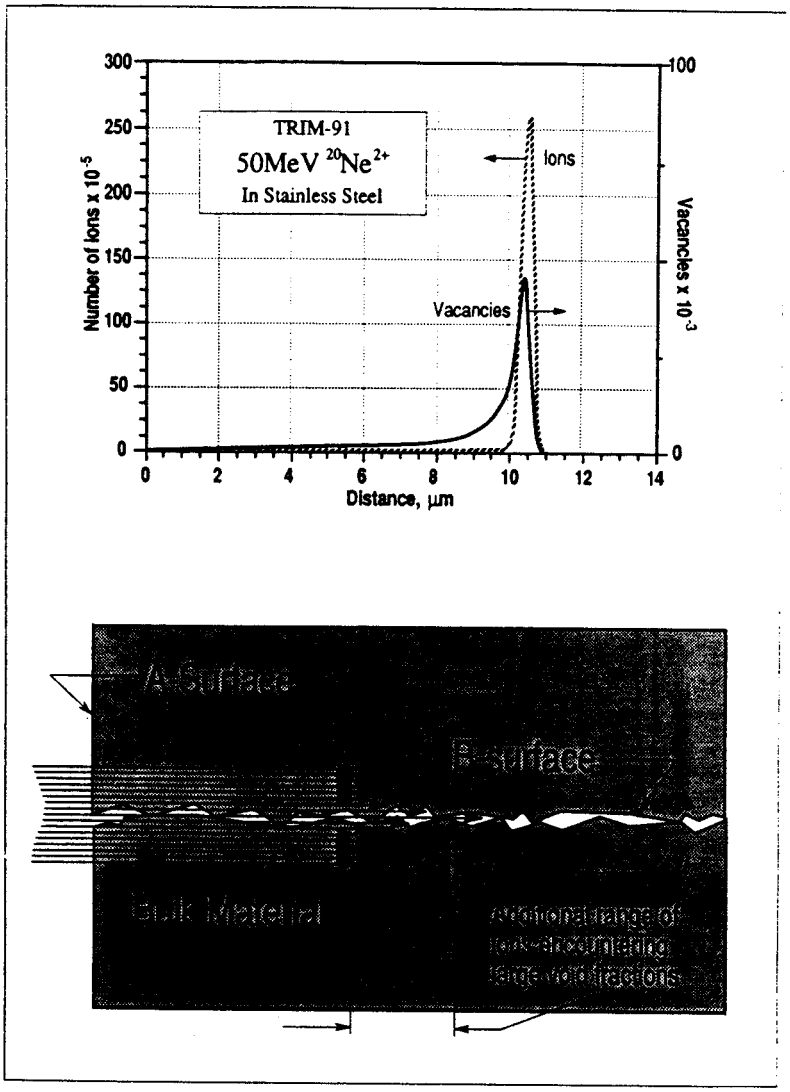


**Figure 1: The upper panel shows predictions by the computer code TRIM-91 of the implanted ion concentration profile and the expected damage profile for 50 MeV $^{20}Ne^{2+}$ ions in stainless steel. The lower panel shows the effect of surface roughness on ion ranges.**

To gain experience with actual wear measurements, we are just completing measurements using activated piston rings in a small engine.[3] A piston ring was activated to 7.5 microCuries of $^{56}Co$ at KfK, Karlsruhe. An 8.5 kW, single cylinder, industrial engine was donated by Briggs and Stratton Corporation. The engine was fitted with an external oil pump to pump oil to an oil reservoir platform. There the oil line contained a lead-shielded copper coil in which a photon detector was placed. This platform is shown in Fig. 3. The efficiency of the photon detector relative to a 3 in. by 3 in. NaI detector at 1.33 MeV was 90%. The detection efficiency for the detector-coil geometry was measured by initially filling the oil coil with thorium chloride, of a known amount and activity, dissolved in water. The engine was then run for over 40 hours. The data for about 40 hours of operation are shown

in Fig. 4. There was a break-in within the first hour, indicated by the large wear rate at the beginning of the test. The power output of the engine was increased from 1.8 kW to 5.6 kW during the test, but, excepting the break-in period, the wear rate remained nearly constant. The head was modified at about 23 hours to increase the compression ratio from 7.6 to 9.5. This modification produced another large increase of short duration in the wear rate, as shown in the figure.

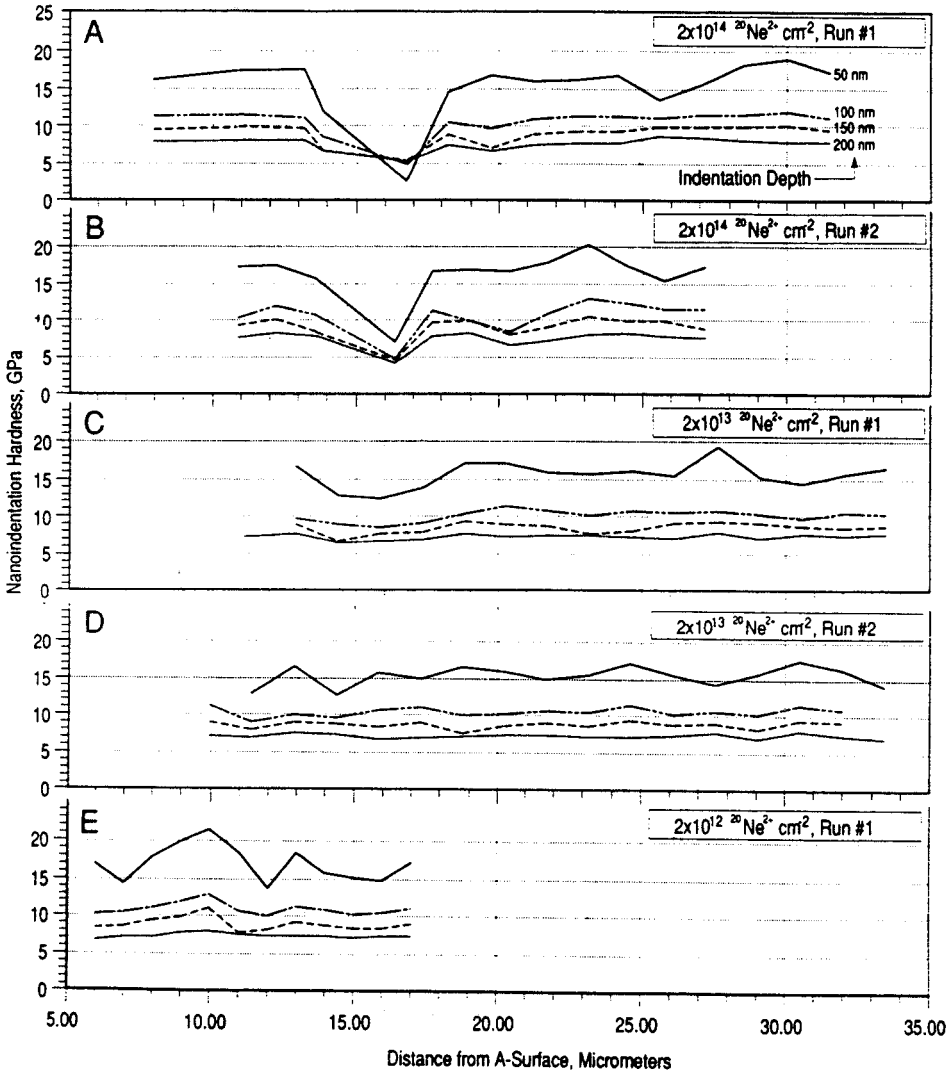


**Figure 2: Nanoindentation hardness profiles are shown of material below the B-surfaces exposed by grinding and polishing.**

The sensitivity of measuring radioactivity in engine oil is quite good. With our system, the integrated wear rate corresponds to an activity of roughly 50 nCi at the end of the test. It is difficult to monitor wear reliably for such small activity losses by measuring the activity of the ring during the test.

Finally, a piston ring wear model has been completed.[4] This model, which has been implemented in a computer simulation, includes ring dynamics, blow-by, and a hydrodynamic lubrication model. This

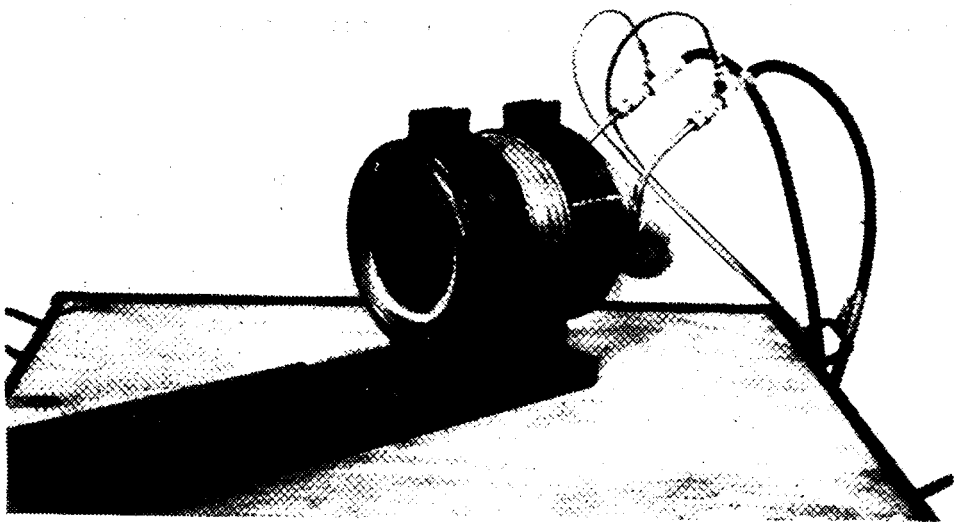

Figure 3: The oil reservoir platform for the engine tests is shown. The copper coil surrounds the cryostat of a high-efficiency photon detector. Lead shielding is also used (not shown).

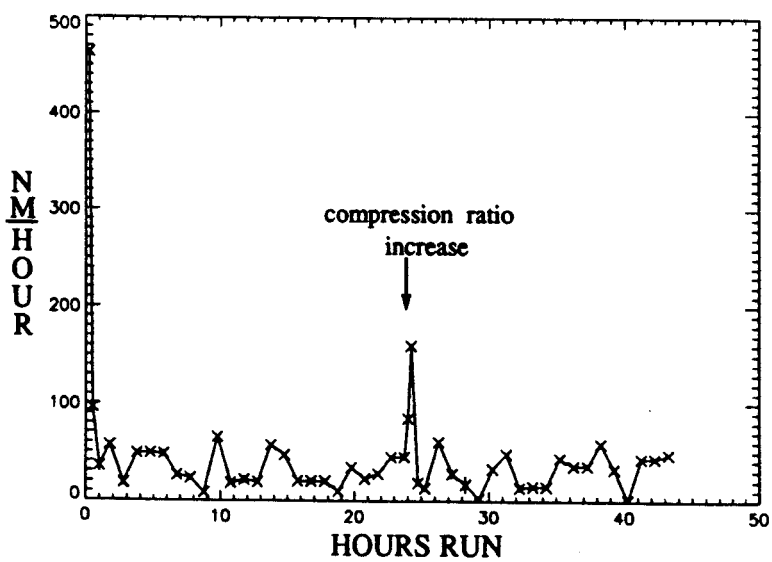


Figure 4: Wear rate data for about 40 hours of engine operation are shown. Large wear rates are observed at the beginning of the test ("break-in" period) and when the compression ratio was increased at 23 hours into the test.

simulation can provide guidence for future tribological testing using surface-layer activation or the radioactive ion implantation technique by allowing one to access order-of-magnitude ring wear for a given set of operating conditions before a test is conducted. This model also provides a framework for analysis of the factors that are responsible for excessive friction, wear, and blow-by.

## References


1. D.S. Grummon, R. Shalek, T. Rachel, H. Schock, R.M. Ronningen, and Wm.C. McHarris, Proceedings of the Symposium on Phase Formation and Modification by Beam-Solid Interactions, Fall Meeting of the Materials Research Society, Boston, MA, December 2-6, 1991.
2. J.P. Biersack and L.G. Haggmark, Nucl. Instr. and Meth.**174**, 257(1980); J.F. Ziegler, private communication.
3. D.A. Barkman, "An Evaluation of the Parameters Involved in Developing a Radioactive Based Wear Diagnostic System," M.S. Thesis, Department of Mechanical Engineering, Michigan State University, East Lansing, MI, July, 1992.
4. Y. Chung, "Development and Analysis of a Fire Ring Wear Model for a Piston Engine," Ph.D. Thesis, Department of Mechanical Engineering, Michigan State University, East Lansing, MI, July, 1992.

# RESEARCH EXPERIENCE FOR UNDERGRADUATES

Wolfgang Bauer

From June 17, 1991, to August 23, 1991, the Department of Physics and Astronomy, College of Natural Science, and the National Superconducting Cyclotron Laboratory, Michigan State University, conducted a Research Experiences for Undergraduates (REU) program. The program was supported jointly by the National Science Foundation and Michigan State University. Nineteen undergraduate students participated in the program, and each student was supervised by a faculty member in the Department of Physics and Astronomy at MSU. The program was run by two MSU faculty members, Assistant Professors M. Dubson and W. Bauer. This was the fifth year in which the Physics/Astronomy Department and the NSCL have run an REU program.

Each of these REU students performed research, wrote a research report and gave a thirty minute research seminar summarizing her/his research project.

The final composition of our selected 19 students was: 8 non-minority male, 8 non-minority female, 2 minority male, and 1 minority female. 6 of these students worked with faculty advisors from the NSCL (2 non-minority males, 2 non-minority females, 1 minority male, and 1 minority female).

| Student | College | Advisor |
|---|---|---|
| Tracie Drew | Grambling State, LA | Wolfgang Bauer, Com. |
| Sally Gaff | Taylor U., IN | Edwin Kashy, Acc. |
| Eyal Goldman | UCLA, CA | Martin Berz, Acc. |
| Jon Kruse | Monmouth, IL | Aaron Galonsky, Nuc. |
| Alice Liu | U. Illinois, IL | B. Alex Brown, Nuc. |
| Lenward Seals | Grambling St., LA | Gary Westfall, Nuc. |

Table 1: REU students and their NSCL advisors.

The students worked on projects in accelerator, computational, and nuclear physics. The following contains a list of the titles of these projects:

- Accelerator Physics
  - Sally Gaff: Simulation of Neutron Pulses for Use in Explosive Detection Systems
  - Eyal Goldmann: The Use of Mirror Image Symmetry for the Elimination of Optical Aberrations

- Computational Physics
  - Tracie Drew: Introductory Physics Labs and Computer Technology
- Nuclear Physics
  - Jon J. Kruse: $^{11}$Li Fragmentation Studies
  - Alice Liu: Shell Effects in Multi-Fermion Systems
  - Lenward T. Seals: Multiwire Proportional Counters